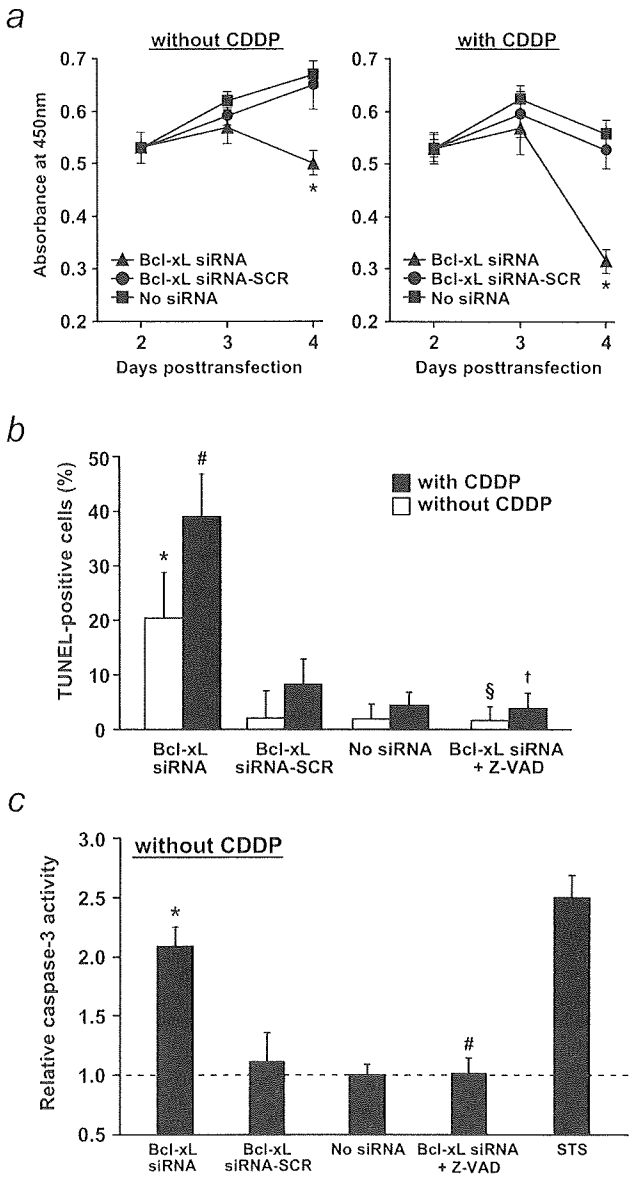

FIGURE 3 – Bcl-xL siRNA inhibited the growth of PC-3 cells and enhanced the cells' sensitivity to CDDP. (*a*) PC-3 cells transfected with Bcl-xL siRNA or Bcl-xL siRNA-SCR were incubated with CDDP (12 μM; right panel) or without (left panel) at 48 hr after transfection. The cell viability was determined at each time point with a cell counting kit. The results represent means ± SD ($n = 8$). *$p <$ 0.001 *versus* Bcl-xL siRNA-SCR. (*b*) PC-3 cells transfected with Bcl-xL siRNA or Bcl-xL siRNA-SCR were treated with CDDP (12 μM, black bars) either alone or in the presence of Z-VAD-FMK (50 μM). TUNEL assay was performed 72 hr later. The results represent means ± SD ($n = 6$). *$p < 0.001$ *versus* Bcl-xL siRNA-SCR without CDDP; #$p < 0.001$ *versus* Bcl-xL siRNA-SCR with CDDP; §$p < 0.001$ *versus* Bcl-xL siRNA without CDDP and †$p < 0.001$ *versus* Bcl-xL siRNA with CDDP. (*c*) PC-3 cells were transfected with Bcl-xL siRNA or Bcl-xL siRNA-SCR and Z-VAD-FMK (50 μM) was added at 6 hr after transfection. Caspase-3 activity was determined 72 hr post-transfection. Caspase-3 activity is shown as relative to that with no siRNA. Staurosporine (STS, 5 μM) was used as a positive control. The results represent means ± SD ($n = 4$). *$p < 0.001$ *versus* Bcl-xL siRNA-SCR; #$p < 0.001$ *versus* Bcl-xL siRNA.

Comparison between combinational treatment of Bcl-xL siRNA/CDDP and CDDP alone

We compared the anti-tumor effect of combinational treatment of Bcl-xL siRNA/CDDP and CDDP (2 or 4 mg/kg) alone. As shown in Fig. 7, a combinational treatment of Bcl-xL siRNA with a low dose of CDDP (2 mg/kg) showed significant inhibition compared with a high dose of CDDP (4 mg/kg) alone ($p < 0.05$).

Atelocollagen enhanced delivery efficiency of siRNA in PC-3 xenografts

Cy3-labeled Bcl-xL siRNA (100 μg) with or without atelocollagen was injected iv into mice bearing PC-3 xenografts. Strong fluorescence intensity was observed in the tumors upon injection of Bcl-xL siRNA-Cy3 with atelocollagen, but almost no fluorescence was observed in the tumors upon injection of a naked Bcl-xL siRNA-Cy3 (Fig. 8*a*). The transfection efficiency of Bcl-xL siRNA-Cy3 in tumors after intravenously injection with or without atelocollagen was 40 and 6%, respectively. To examine the locations of systemically delivered Bcl-xL siRNA-Cy3 with atelocollagen in the tumors, sections were stained for endothelium (CD31) and fibroblasts (FSP-1), respectively. Some spots of red fluorescence of Bcl-xL siRNA-Cy3 were merged with CD31- or fibroblast-specific protein-1- positive cells (Figs. 8*b*, 8*c*).

Distribution of siRNA in PC-3 xenografts and several normal organs after systemic administration via *atelocollagen*

To investigate the distribution of siRNA *in vivo*, we intravenously injected nude mice bearing PC-3 xenografts with Bcl-xL siRNA/atelocollagen, and then analyzed the amounts of siRNA in several tissues by hybridization with a specific probe followed by reverse-phase HPLC analysis. As shown in Figures 9*a* and 9*b*, both reliable reproducibility and satisfactory recovery of the measurement were obtained. The xenografts and several normal organs (liver, kidney, lung, spleen and brain) were excised at the indicated time points after siRNA injection. The results showed 12.4, 10.4 and 2.6 ng (average amounts from four tumors) of intact Bcl-xL siRNA per gram of tissue in PC-3 xenografts excised 15, 30 and 60 min after injection, respectively. No intact siRNA was found in the normal tissues analyzed (Fig. 9*c*).

No IFN-α induction was found in pDCs after treatment with Bcl-xL siRNA in vitro

The IFN-α level in the medium of pDCs was examined 24 hr after the treatment with Bcl-xL siRNA with or without atelocollagen. No IFN-α induction was found in the cells treated with either a naked Bcl-xL siRNA or Bcl-xL siRNA with atelocollagen, whereas IFN-α induction was found in the medium treated with positive control poly(I:C) (Fig. 10*a*).

No abnormality was found in the IFN-α induction, liver enzyme or renal function of nude mice after systemic administration with Bcl-xL siRNA

The IFN-α level in serum was examined in mice injected with 100 μg of Bcl-xL siRNA in the presence or absence of atelocollagen. Neither naked Bcl-xL siRNA nor Bcl-xL siRNA with atelocollagen induced IFN-α, whereas positive control poly(I:C) strongly induced it (Fig. 10*b*). Liver and renal functions were tested at days 1 and 7 after treatment with Bcl-xL siRNA/atelocollagen only or Bcl-xL siRNA/atelocollagen plus CDDP, respectively. Neither liver damage (AST and ALT) nor renal damage (BUN and creatinine) was observed after treatment with Bcl-xL siRNA/atelocollagen or Bcl-xL siRNA/atelocollagen plus CDDP, whereas positive control, CCl_4 caused serious liver damage at day 1 (Fig. 10*c*).

Discussion

RNAi *in vivo* has tremendous potential, not only for the elucidation of gene function in animals but also as a therapeutic platform

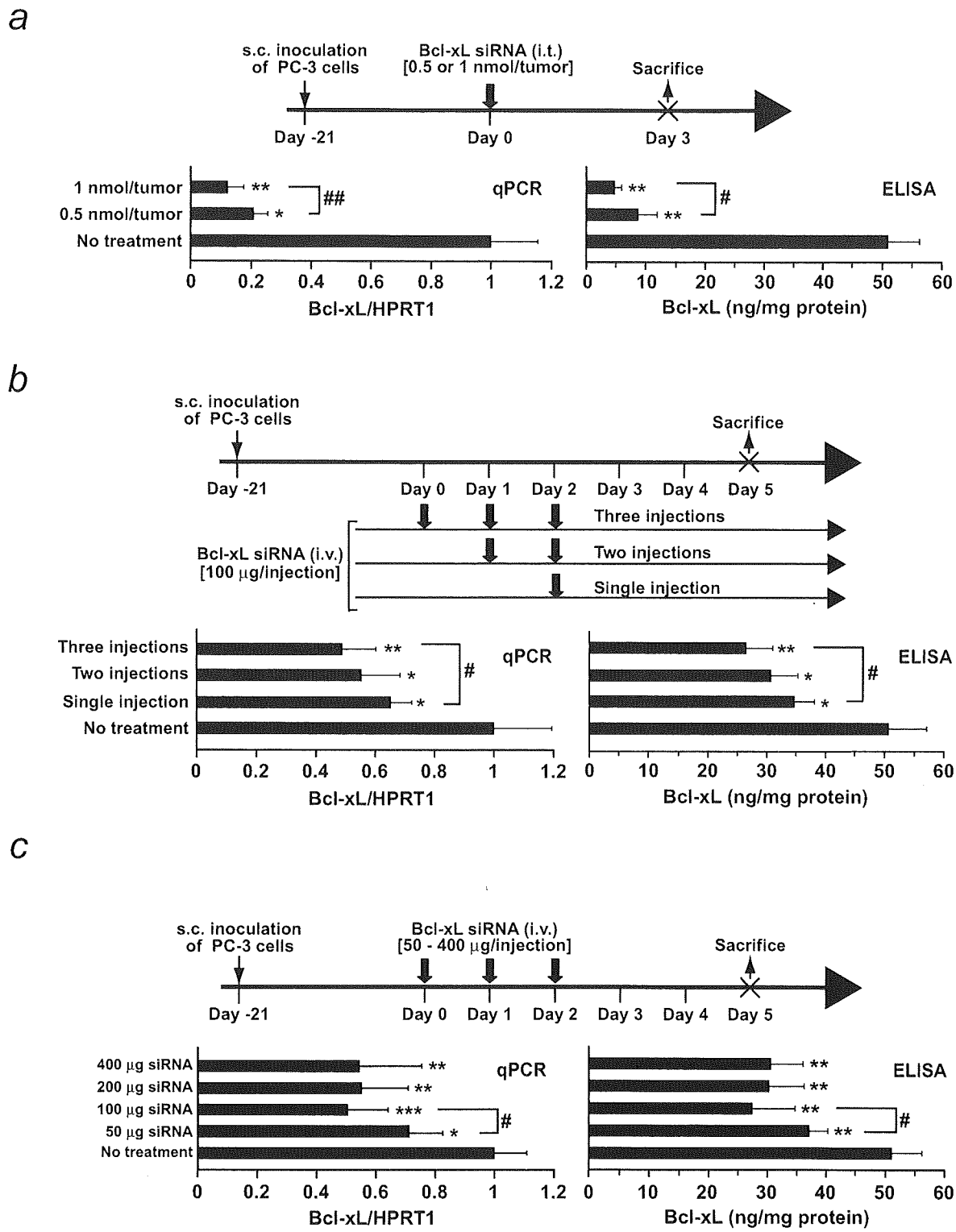

FIGURE 4 – Determination of an optimal concentration and injection mode of Bcl-xL siRNA for *in vivo* therapeutic experiments. (*a*) Bcl-xL siRNA (0.5 or 1 nmol/tumor) with 0.5% atelocollagen was injected into PC-3 xenografts. Mice were killed and the tumors were excised after 3 days following one injection of Bcl-xL siRNA. The mRNA and protein levels of Bcl-xL were determined by real-time PCR and ELISA, respectively. The results represent means ± SD ($n = 4$). $^{*}p < 0.01$; $^{**}p < 0.001$ *versus* no treatment. $^{\#}p < 0.05$; $^{\#\#}p < 0.01$ versus 0.5 nmol/tumor. (*b, c*) Mice bearing PC-3 xenografts (tumor volume = 50–80 mm^3) were systemically injected with Bcl-xL siRNA/atelocollagen into the tail vein. Three days after the last injection, the mice were killed and the tumors were excised. The mRNA and protein levels of Bcl-xL were determined by real-time PCR and ELISA, respectively. (*b*) Bcl-xL siRNA (100 μg) with one injection, 2 consecutive injections, or 3 consecutive injections was administered, respectively. The results represent means ± SD ($n = 3$). $^{*}p < 0.05$; $^{**}p < 0.01$ *versus* no treatment. $^{\#}p < 0.05$ versus single injection. (*c*) Three consecutive injections with various concentrations of Bcl-xL siRNA were examined. The results represent means ± SD ($n = 4$). $^{*}p < 0.05$; $^{**}p < 0.01$; $^{***}p < 0.001$ *versus* no treatment. $^{\#}p < 0.05$. HPRT1 was used as a control.

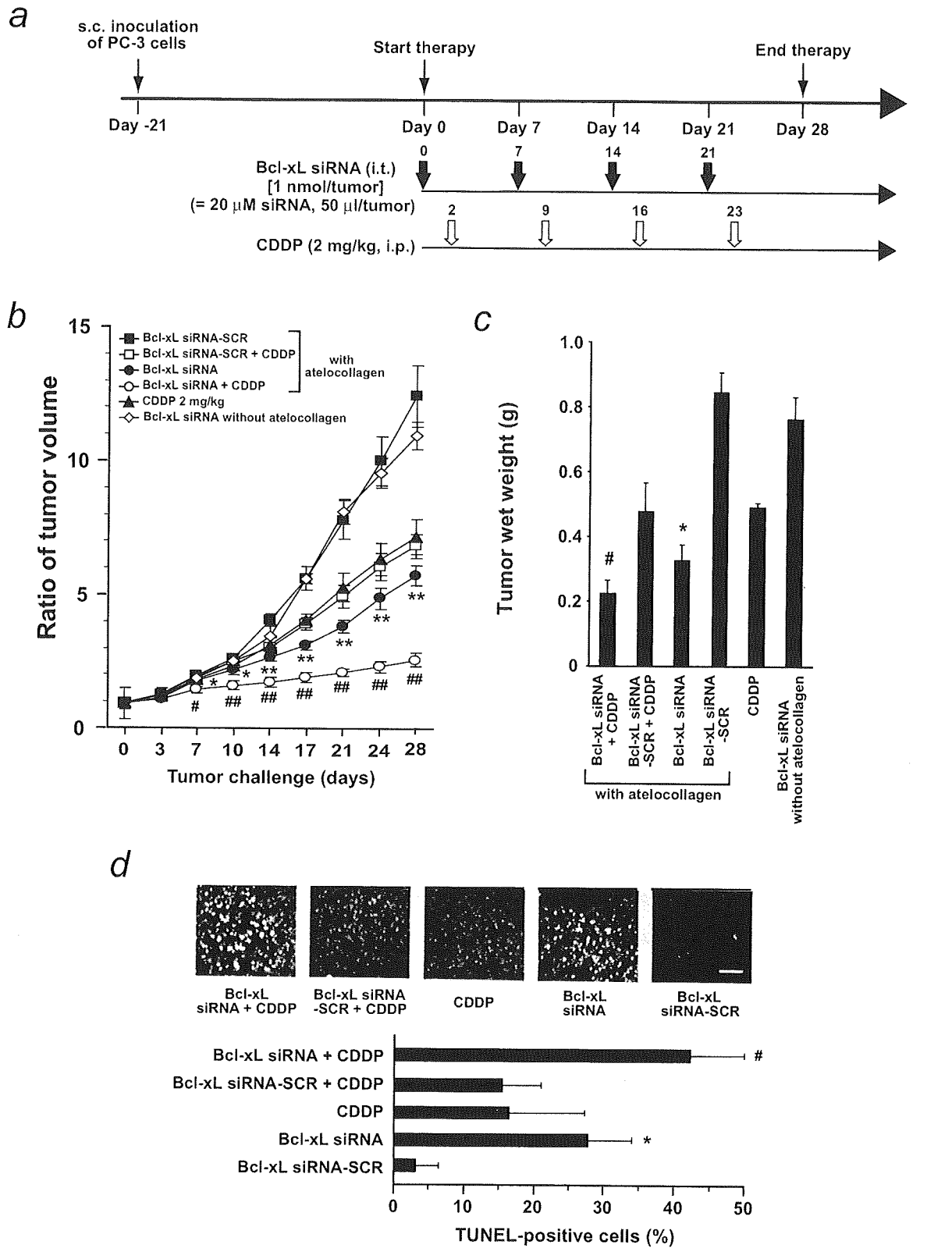

FIGURE 5 – Anticancer effect of local administration of Bcl-xL siRNA in combination with CDDP in PC-3 xenografts. (*a*) Procedure for therapeutic experiments. (*b*) Tumor growth curves. $^{*}p < 0.05$; $^{**}p < 0.001$ *versus* Bcl-xL siRNA-SCR. $^{\#}p < 0.05$; $^{\#\#}p < 0.001$ versus Bcl-xL siRNA-SCR plus CDDP. (*c*) Tumor weights. The tumors were excised and weighed on day 28. $^{*}p < 0.01$ *versus* Bcl-xL siRNA-SCR. $^{\#}p < 0.001$ *versus* Bcl-xL siRNA-SCR plus CDDP. (*d*) TUNEL staining. Results are shown as ratios of TUNEL-positive cells and total cells. $^{*}p < 0.001$ *versus* Bcl-xL siRNA-SCR. $^{\#}p < 0.001$ *versus* Bcl-xL siRNA-SCR plus CDDP. Bar, 100 μm. From (*b*) to (*d*), the results represent means ± SE ($n = 6$).

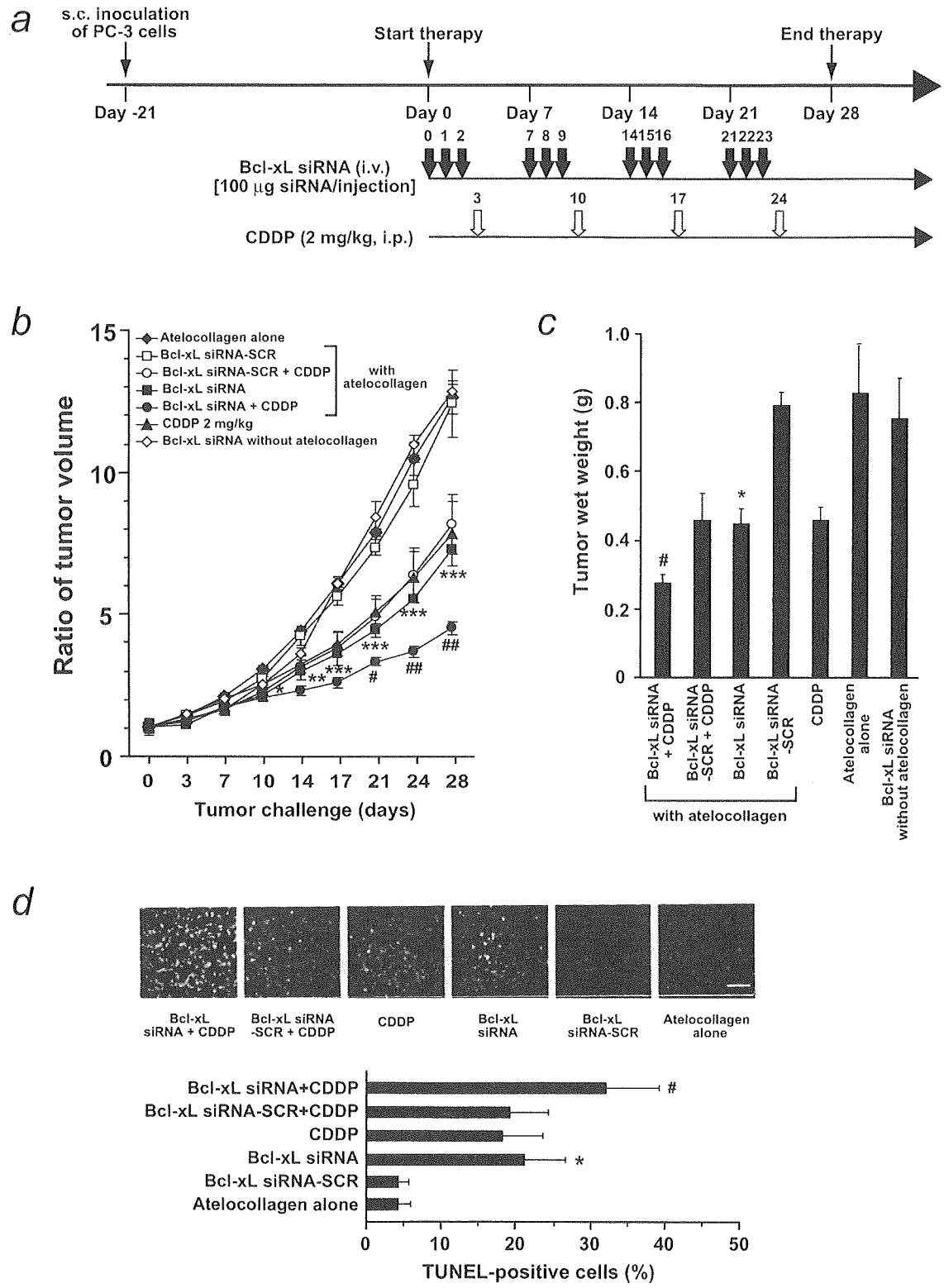

FIGURE 6 – Anticancer effect of systemic administration of Bcl-xL siRNA in combination with CDDP in PC-3 xenografts. (*a*) Procedure for therapeutic experiments. (*b*) Tumor growth curves. $^{*}p < 0.05$; $^{**}p < 0.01$; $^{***}p < 0.001$ *versus* Bcl-xL siRNA-SCR. $^{\#}p < 0.05$; $^{\#\#}p < 0.01$ *versus* Bcl-xL siRNA-SCR plus CDDP. (*c*) Tumor weights. The tumors were excised and weighed on day 28. $^{*}p < 0.001$ *versus* Bcl-xL siRNA-SCR. $^{\#}p < 0.01$ *versus* Bcl-xL siRNA-SCR plus CDDP. (*d*) TUNEL staining. Results are shown as ratios of TUNEL-positive cells and total cells. $^{*}p < 0.001$ *versus* Bcl-xL siRNA-SCR. $^{\#}p < 0.01$ *versus* Bcl-xL siRNA-SCR plus CDDP. Bar, 100 μm. From (*b*) to (*d*), the results represent means ± SE ($n = 6$).

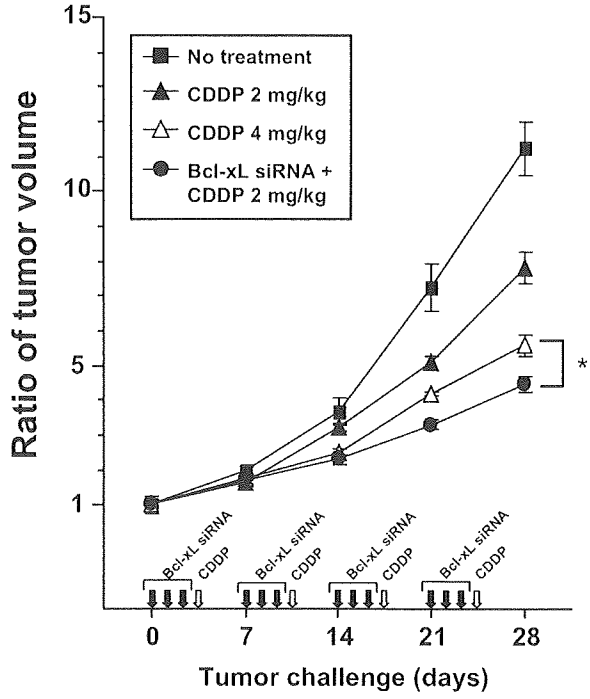

FIGURE 7 – Comparison between a combined treatment of Bcl-xL siRNA/atelocollagen plus CDDP and CDDP alone. The injection intervals of Bcl-xL siRNA with atelocollagen and CDDP were shown in the figure. The results represent means ± SE ($n = 6$). *$p < 0.05$.

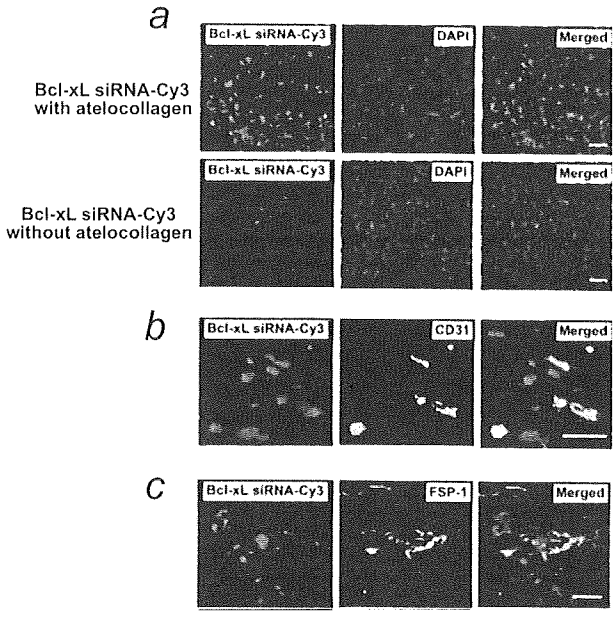

FIGURE 8 – Delivery efficiency of Cy3-labeled Bcl-xL siRNA in PC-3 xenografts. Nude mice bearing xenografts were intravenously injected with 100 μg of Cy3-labeled Bcl-xL siRNA with or without atelocollagen. PC-3 xenografts were excised 24 hr later. Sections were made and the fluorescence was observed. (*a–c*) Sections were stained for nuclei with DAPI (*a*), endothelial cells with CD31 (*b*) and fibroblasts with S100A4/FSP-1 (*c*), respectively. All bars, 20 μm.

in humans.[38] However, there are many obstacles to overcome to apply it therapeutically. Intravenous administration of siRNA in animals results in the rapid, extensive removal of siRNA from the blood *via* renal excretion, tissue distribution, and nuclease degradation.[38] A specific and effective cellular uptake of siRNA in the desired tissues also can be expected. In this study, we determined a modality for delivering siRNA targeting Bcl-xL into pregrown PC-3 xenografts *via* an atelocollagen-mediated systemic administration method, and consequently achieved a significant therapeutic effect. To downregulate Bcl-xL protein effectively in the xenografts, we showed the following modality (Fig. 4), *i.e.*, three consecutive daily *iv* injections of siRNA/atelocollagen complex (siRNA, 100 μg per injection; atelocollagen, 0.05% and 200 μl per single injection). We designated these three consecutive injections as one set, and administered a total of four sets in 4 weeks (Fig. 6*a*).

Atelocollagen is a natural product prepared from bovine dermal collagen.[17] Atelocollagen shows neither antigenicity nor toxicity in animals, since antigenic telopeptides are eliminated by pepsin digestion.[17] The atelocollagen delivery method does not require any chemical modification of the siRNA itself to stabilize it against nuclease, whereas many reports reveal the necessity of chemically modifying siRNA, including changes to the phosphorothioate backbone,[5,39] 2′-*O*-methyl RNA, 2′-deoxy-2′-fluorouri-

a

Reproducibility of the measurement

No.	Times of measurement	Mean ± SD	Coefficient value (%)
Sample 1	3	5.5 ± 0.7	12.7
Sample 2	3	17.5 ± 0.5	2.9
Sample 3	3	33.5 ± 0.8	2.4
Sample 4	3	48.6 ± 1.6	3.3

b

Recovery of the measurement

No.	Endogenous siRNA (ng)	Exogenous siRNA added (ng)	Increased siRNA (ng)	Recovery (%)
Sample 1	4.8	10	12.0	120
Sample 2	17.0	10	10.4	104
Sample 3	33.0	10	9.7	97
Sample 4	47.6	10	9.5	95

c

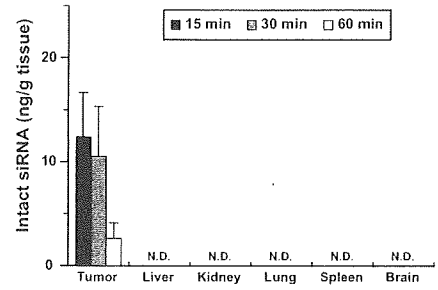

FIGURE 9 – Distribution of siRNA systemically delivered with atelocollagen in xenografts and normal tissues. (*a*) Reproducibility of the measurement. Amount of Bcl-xL siRNA in each tumor sample was repeatedly measured ($n = 3$). Each coefficient value (%) was calculated. (*b*) Recovery of the measurement. Ten nanograms of Bcl-xL siRNA were exogenously added into each tumor sample. The amount of increased siRNA in the sample was measured, and the recovery value was calculated. (*c*) Nude mice bearing xenografts were systemically injected with 100 μg of Bcl-xL siRNA with atelocollagen. PC-3 xenografts and several normal organs (liver, kidney, lung, spleen and brain) were excised 15, 30, or 60 min later. Intact Bcl-xL siRNA in tissues was determined by hybridizing with a specific fluorescence-labeled oligoribonucleotide, followed by quantification with reverse-phase HPLC. The results represent means ± SE ($n = 4$).

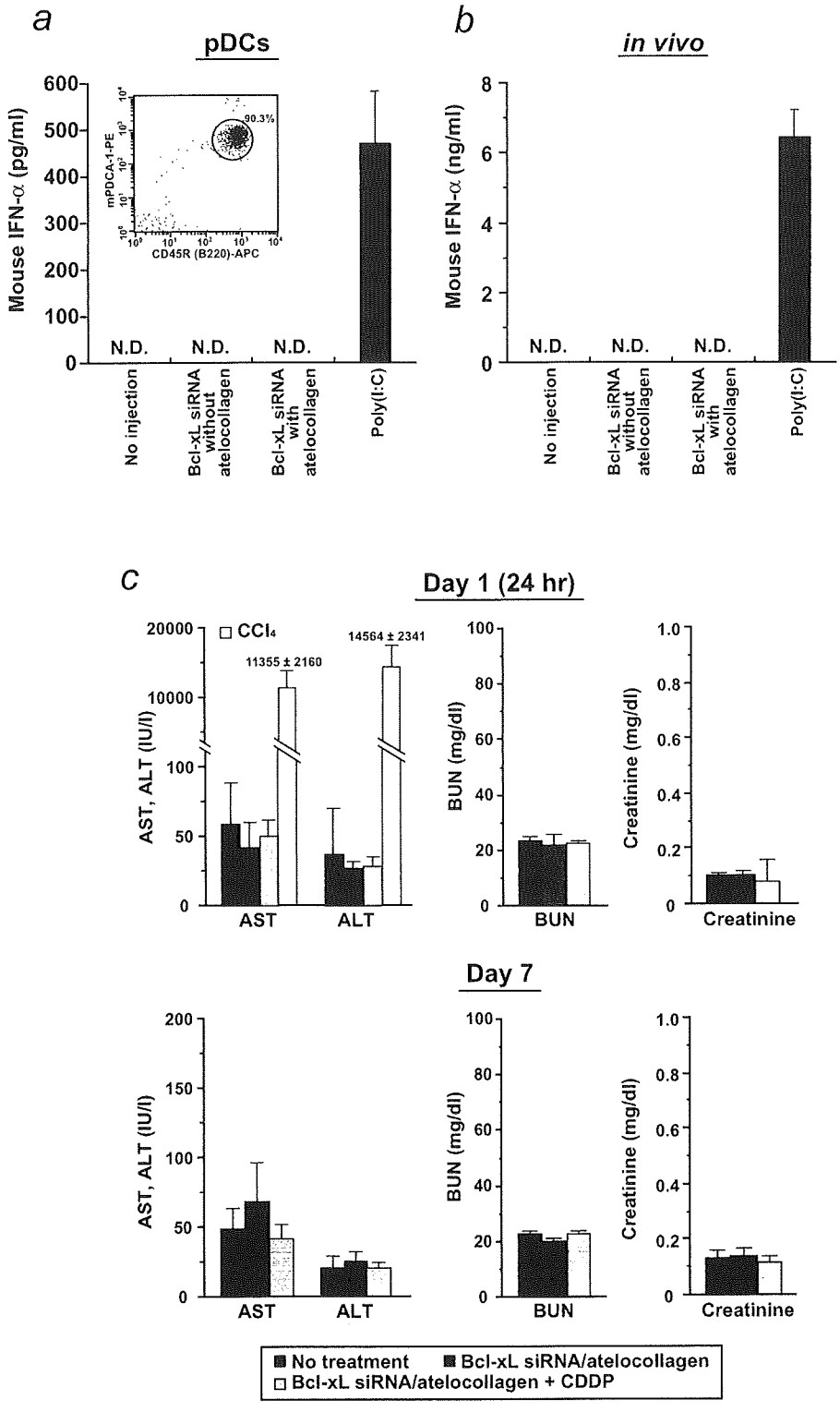

FIGURE 10 – No adverse effect in IFN-α induction or liver enzyme renal function was observed after treatment with Bcl-xL siRNA in pDCs or in nude mice. (*a*) pDCs were incubated with 50 μg/ml of Bcl-xL siRNA with or without atelocollagen. Each medium was harvested 24 hr later. Mouse IFN-α concentration was determined by ELISA. The positive control group was treated with 50 μg/ml of poly(I:C). (*b*) Nude mice were injected with 100 μg of Bcl-xL siRNA with or without atelocollagen into the tail vein. Blood was harvested 6 hr after injection. Mouse IFN-α concentration was determined by ELISA. The positive control group was injected with 100 μg of poly(I:C). (*c*) Bcl-xL siRNA/atelocollagen complex (100 μg) was intravenously injected followed by CDDP (2 mg/kg) injection into nude mice. Blood was collected at the indicated days. The levels of AST, ALT, BUN, and creatinine were measured. CCl_4 was used as a positive control for acute liver damage. The results represent means ± SD (n = 3).

dine RNA, or locked nucleic acid.[39,40] These chemical modifications, especially that involving the phosphorothioate backbone, cause toxicity in animals. On the other hand, when we intravenously injected mice with the Bcl-xL siRNA/atelocollagen complex, we observed no liver or renal toxicity. Moreover, there was no IFN-α induction in mice. No gross adverse effects, *i.e.*, loss of body weight, were observed during the therapy (data not shown). Therefore, the proposed therapeutic procedure is safe.

The amounts of Bcl-xL siRNA in tumors intravenously administered *via* atelocollagen were successfully detected. In contrast, we did not detect any intact Bcl-xL siRNA in brain, liver, or spleen at all. These results strongly suggested that the systemic administration method *via* atelocollagen is very selective in delivery and accumulation in tumor tissues, consistent with the report[23] using luciferase siRNA and *in vivo* imaging system. This phenomenon is probably because of the enhanced permeability

and retention (EPR) effect.[41] High molecular weight macromolecules (more than 40 kDa) show restricted renal excretion and prolonged plasma half-lives.[42] Macromolecules' prolonged circulation time enables them to utilize the abnormal vasculature with increased permeability found in solid tumors. Indeed, the PC-3 xenograft abundantly expresses vascular endothelial growth factor-A (VEGF-A contents in the PC-3 xenograft: 103 ± 16 pg/mg protein; means ± SD from four xenografts),[34] and thus VEGF-A upregulates the tumor permeability.[43] Moreover, we also successfully enabled the delivery of siRNA with atelocollagen intravenously to inflammatory tissues *via* a similar EPR effect.[16] In the inflammatory tissues, MCP-1 upregulates the permeability.[16,44,45] From a viewpoint of enhanced permeability, tumors and inflammatory tissues resemble each other. Therefore, the atelocollagen-mediated systemic method enables to deliver the siRNA specifically into either tumors or inflammatory tissues.

The *Bcl-x* gene codes two transcript variants (Bcl-xL, long isoform; and Bcl-xS, short isoform; respectively) by alternative splicing.[46] Bcl-xL shows anti-apoptotic activity, whereas that of Bcl-xS is pro-apoptotic. There is a difference of only 189 continuous nucleotides (as shown in a black frame in Fig. 1*a*) between Bcl-xL and Bcl-xS, and Bcl-xL possesses all of the sequences that Bcl-xS has. Because of the opposite activity of the two variants, we designed a specific siRNA to downregulate only Bcl-xL. Thus, we selected all of the target sequence for the siRNAs within the region that only Bcl-xL possesses, and we demonstrated a specific decrease in the expression of Bcl-xL upon transfection of Bcl-xL siRNA into PC-3 cells without any changes in the expression of Bcl-xS (Fig. 2*c*). So far, although many reports have shown Bcl-xL targeting cancer therapy *via* either an antisense or RNAi strategy, few reports have dealt carefully with the issue of Bcl-xS. It is crucial to design a specific siRNA when the target gene possesses several transcript variants, especially for a gene that shows different activity upon coding.

In prostate cancer, chemotherapeutics such as paclitaxel (Taxol, PTX) and CDDP have a long history of use and provide a great degree of clinical benefit.[47] In our previous report,[15] we showed the combined anticancer effect of siRNA targeting midkine (MK) and PTX against PC-3 xenograft. MK is a heparin-binding growth factor that promotes the cell cycle in cancer cells.[10,11,48] We successfully enabled PTX dose reductions of up to 12 mg/kg without loss of the antitumor effect, when combined with MK siRNA *via* the atelocollagen-mediated local delivery method.[15] At a dose of 12 mg/kg, we observed no severe bone marrow suppression (leukopenia and neutropenia). The principal mechanism underlying PTX's cytotoxic action is the stabilization of microtubules, which leads to mitotic arrest.[49] PTX has also been shown to induce phosphorylation of Bcl-xL protein as well as Bcl-2, leading to apoptosis.[50,51] Thus, the abundant expression of Bcl-xL is a crucial determinant of PTX chemotherapy efficacy, and reduced expression of Bcl-xL *via* RNAi can weaken PTX's anticancer effect. Accordingly, we chose CDDP as a chemotherapeutic agent to combine with Bcl-xL siRNA therapy. We were able to reduce the CDDP dose as much as 2 mg/kg by combining it with Bcl-xL siRNA therapy.

In conclusion, we established an atelocollagen-mediated siRNA delivery method *via* systemic administration to treat pregrown solid xenografts of prostate cancer without any severe side effects. Using the proposed method, we enabled intact siRNA to accumulate selectively in tumors. This method has the potential to become a conclusive method to systemically deliver siRNA to animals.

Acknowledgments

The authors thank Ms. Sachiko Fukuda and Dr. Dongliang Cao for their excellent technical assistance. We also thank Drs Kazuo Kita, Ichiro Fujimoto, Ryoichi Ioka, and Yasushi Matsuki for helpful suggestions for the experiments and the manuscript.

References

1. Fire A, Xu S, Montgomery MK, Kostas SA, Driver SE, Mello CC. Potent and specific genetic interference by double-stranded RNA in *Caenorhabditis elegans*. Nature 1998;391:806–11.
2. Elbashir SM, Harborth J, Lendeckel W, Yalcin A, Weber K, Tuschl T. Duplexes of 21-nucleotide RNAs mediate RNA interference in cultured mammalian cells. Nature 2001;411:494–8.
3. Ryther RC, Flynt AS, Phillips JA, 3rd, Patton JG. siRNA therapeutics: big potential from small RNAs. Gene Ther 2005;12:5–11.
4. Reischl D, Zimmer A. Drug delivery of siRNA therapeutics: potentials and limits of nanosystems. Nanomedicine 2008;5:8–20.
5. Kawakami S, Hashida M. Targeted delivery systems of small interfering RNA by systemic administration. Drug Metab Pharmacokinet 2007;22:142–51.
6. McCaffrey AP, Meuse L, Pham TT, Conklin DS, Hannon GJ, Kay MA. RNA interference in adult mice. Nature 2002;418:38–9.
7. Santel A, Aleku M, Keil O, Endruschat J, Esche V, Durieux B, Loffler K, Fechtner M, Rohl T, Fisch G, Dames S, Arnold W, et al. RNA interference in the mouse vascular endothelium by systemic administration of siRNA-lipoplexes for cancer therapy. Gene Ther 2006; 13:1360–70.
8. Urban-Klein B, Werth S, Abuharbeid S, Czubayko F, Aigner A. RNAi-mediated gene-targeting through systemic application of polyethylenimine (PEI)-complexed siRNA in vivo. Gene Ther 2005;12: 461–6.
9. Juliano R, Alam MR, Dixit V, Kang H. Mechanisms and strategies for effective delivery of antisense and siRNA oligonucleotides. Nucleic Acids Res 2008;36:4158–71.
10. Takei Y, Kadomatsu K, Matsuo S, Itoh H, Nakazawa K, Kubota S, Muramatsu T. Antisense oligodeoxynucleotide targeted to Midkine, a heparin-binding growth factor, suppresses tumorigenicity of mouse rectal carcinoma cells. Cancer Res 2001;61:8486–91.
11. Takei Y, Kadomatsu K, Itoh H, Sato W, Nakazawa K, Kubota S, Muramatsu T. 5′-,3′-inverted thymidine-modified antisense oligodeoxynucleotide targeting midkine. Its design and application for cancer therapy. J Biol Chem 2002;277:23800–6.
12. Hanai K, Kurokawa T, Minakuchi Y, Maeda M, Nagahara S, Miyata T, Ochiya T, Sano A. Potential of atelocollagen-mediated systemic antisense therapeutics for inflammatory disease. Hum Gene Ther 2004;15:263–72.
13. Takei Y, Kadomatsu K, Yuasa K, Sato W, Muramatsu T. Morpholino antisense oligomer targeting human midkine: its application for cancer therapy. Int J Cancer 2005;114:490–7.
14. Takei Y, Kadomatsu K, Yuzawa Y, Matsuo S, Muramatsu T. A small interfering RNA targeting vascular endothelial growth factor as cancer therapeutics. Cancer Res 2004;64:3365–70.
15. Takei Y, Kadomatsu K, Goto T, Muramatsu T. Combinational antitumor effect of siRNA against midkine and paclitaxel on growth of human prostate cancer xenografts. Cancer 2006;107:864–73.
16. Ishimoto T, Takei Y, Yuzawa Y, Hanai K, Nagahara S, Tarumi Y, Matsuo S, Kadomatsu K. Downregulation of monocyte chemoattractant protein-1 involving short interfering RNA attenuates hapten-induced contact hypersensitivity. Mol Ther 2008;16:387–95.
17. Ochiya T, Takahama Y, Nagahara S, Sumita Y, Hisada A, Itoh H, Nagai Y, Terada M. New delivery system for plasmid DNA in vivo using atelocollagen as a carrier material: the Minipellet. Nat Med 1999;5:707–10.
18. Hanai K, Takeshita F, Honma K, Nagahara S, Maeda M, Minakuchi Y, Sano A, Ochiya T. Atelocollagen-mediated systemic DDS for nucleic acid medicines. Ann N Y Acad Sci 2006;1082:9–17.
19. Minakuchi Y, Takeshita F, Kosaka N, Sasaki H, Yamamoto Y, Kouno M, Honma K, Nagahara S, Hanai K, Sano A, Kato T, Terada M, et al. Atelocollagen-mediated synthetic small interfering RNA delivery for effective gene silencing in vitro and in vivo. Nucleic Acids Res 2004;32:e109.
20. Takei Y, Kadomatsu K. In vivo delivery technique of nucleic acid compounds using atelocollagen: its use in cancer therapeutics targeted at the heparin-binding growth factor midkine. Gene Ther Mol Biol 2005;9:257–64.
21. Fujii T, Saito M, Iwasaki E, Ochiya T, Takei Y, Hayashi S, Ono A, Hirao N, Nakamura M, Kubushiro K, Tsukazaki K, Aoki D. Intratumor injection of small interfering RNA-targeting human papillomavirus 18 E6 and E7 successfully inhibits the growth of cervical cancer. Int J Oncol 2006;29:541–8.
22. Hirai K, Sasaki H, Sakamoto H, Takeshita F, Asano K, Kubota Y, Ochiya T, Terada M. Antisense oligodeoxynucleotide against HST-1/FGF-4 suppresses tumorigenicity of an orthotopic model for human germ cell tumor in nude mice. J Gene Med 2003;5:951–7.
23. Takeshita F, Minakuchi Y, Nagahara S, Honma K, Sasaki H, Hirai K, Teratani T, Namatame N, Yamamoto Y, Hanai K, Kato T, Sano A,

et al. Efficient delivery of small interfering RNA to bone-metastatic tumors by using atelocollagen in vivo. Proc Natl Acad Sci USA 2005;102:12177–82.
24. Makin G, Dive C. Apoptosis and cancer chemotherapy. Trends Cell Biol 2001;11:S22–6.
25. Yamanaka K, Rocchi P, Miyake H, Fazli L, Vessella B, Zangemeister-Wittke U, Gleave ME. A novel antisense oligonucleotide inhibiting several antiapoptotic Bcl-2 family members induces apoptosis and enhances chemosensitivity in androgen-independent human prostate cancer PC3 cells. Mol Cancer Ther 2005;4:1689–98.
26. Castilla C, Congregado B, Chinchon D, Torrubia FJ, Japon MA, Saez C. Bcl-xL is overexpressed in hormone-resistant prostate cancer and promotes survival of LNCaP cells via interaction with proapoptotic Bak. Endocrinology 2006;147:4960–7.
27. Lebedeva I, Rando R, Ojwang J, Cossum P, Stein CA. Bcl-xL in prostate cancer cells: effects of overexpression and down-regulation on chemosensitivity. Cancer Res 2000;60:6052–60.
28. Li X, Marani M, Mannucci R, Kinsey B, Andriani F, Nicoletti I, Denner L, Marcelli M. Overexpression of BCL-X(L) underlies the molecular basis for resistance to staurosporine-induced apoptosis in PC-3 cells. Cancer Res 2001;61:1699–706.
29. Zhu H, Guo W, Zhang L, Davis JJ, Teraishi F, Wu S, Cao X, Daniel J, Smythe WR, Fang B. Bcl-XL small interfering RNA suppresses the proliferation of 5-fluorouracil-resistant human colon cancer cells. Mol Cancer Ther 2005;4:451–6.
30. Bai J, Sui J, Demirjian A, Vollmer CM, Jr, Marasco W, Callery MP. Predominant Bcl-XL knockdown disables antiapoptotic mechanisms: tumor necrosis factor-related apoptosis-inducing ligand-based triple chemotherapy overcomes chemoresistance in pancreatic cancer cells in vitro. Cancer Res 2005;65:2344–52.
31. Zhang L, Zhao H, Sun A, Lu S, Liu B, Tang F, Feng Y, Zhao L, Yang R, Han ZC. Early down-regulation of Bcl-xL expression during megakaryocytic differentiation of thrombopoietin-induced CD34+ bone marrow cells in essential thrombocythemia. Haematologica 2004;89:1199–206.
32. Komuro I, Yasuda T, Iwamoto A, Akagawa KS. Catalase plays a critical role in the CSF-independent survival of human macrophages via regulation of the expression of BCL-2 family. J Biol Chem 2005;280:41137–45.
33. Ohga S, Nomura A, Takada H, Tanaka T, Furuno K, Takahata Y, Kinukawa N, Fukushima N, Imai S, Hara T. Dominant expression of interleukin-10 and transforming growth factor-beta genes in activated T-cells of chronic active Epstein-Barr virus infection. J Med Virol 2004;74:449–58.
34. Takei Y, Nemoto T, Mu P, Fujishima T, Ishimoto T, Hayakawa Y, Yuzawa Y, Matsuo S, Muramatsu T, Kadomatsu K. In vivo silencing of a molecular target by short interfering RNA electroporation: tumor vascularization correlates to delivery efficiency. Mol Cancer Ther 2008;7:211–21.
35. Cao W, Manicassamy S, Tang H, Kasturi SP, Pirani A, Murthy N, Pulendran B. Toll-like receptor-mediated induction of type I interferon in plasmacytoid dendritic cells requires the rapamycin-sensitive PI(3)K-mTOR-p70S6K pathway. Nat Immunol 2008;9:1157–64.
36. Allman D, Dalod M, Asselin-Paturel C, Delale T, Robbins SH, Trinchieri G, Biron CA, Kastner P, Chan S. Ikaros is required for plasmacytoid dendritic cell differentiation. Blood 2006;108:4025–34.
37. Kwon YH, Jovanovic A, Serfas MS, Tyner AL. The Cdk inhibitor p21 is required for necrosis, but it inhibits apoptosis following toxin-induced liver injury. J Biol Chem 2003;278:30348–55.
38. White PJ. Barriers to successful delivery of short interfering RNA after systemic administration. Clin Exp Pharmacol Physiol 2008;35:1371–6.
39. Watts JK, Deleavey GF, Damha MJ. Chemically modified siRNA: tools and applications. Drug Discov Today 2008;13:842–55.
40. Braasch DA, Jensen S, Liu Y, Kaur K, Arar K, White MA, Corey DR. RNA interference in mammalian cells by chemically-modified RNA. Biochemistry 2003;42:7967–75.
41. Satchi-Fainaro R, Puder M, Davies JW, Tran HT, Sampson DA, Greene AK, Corfas G, Folkman J. Targeting angiogenesis with a conjugate of HPMA copolymer and TNP-470. Nat Med 2004;10:255–61.
42. Greish K, Fang J, Inutsuka T, Nagamitsu A, Maeda H. Macromolecular therapeutics: advantages and prospects with special emphasis on solid tumour targeting. Clin Pharmacokinet 2003;42:1089–105.
43. Senger DR, Galli SJ, Dvorak AM, Perruzzi CA, Harvey VS, Dvorak HF. Tumor cells secrete a vascular permeability factor that promotes accumulation of ascites fluid. Science 1983;219:983–5.
44. Stamatovic SM, Keep RF, Kunkel SL, Andjelkovic AV. Potential role of MCP-1 in endothelial cell tight junction 'opening': signaling via Rho and Rho kinase. J Cell Sci 2003;116:4615–28.
45. Lee YR, Liu MT, Lei HY, Liu CC, Wu JM, Tung YC, Lin YS, Yeh TM, Chen SH, Liu HS. MCP-1, a highly expressed chemokine in dengue haemorrhagic fever/dengue shock syndrome patients, may cause permeability change, possibly through reduced tight junctions of vascular endothelium cells. J Gen Virol 2006;87:3623–30.
46. Boise LH, Gonzalez-Garcia M, Postema CE, Ding L, Lindsten T, Turka LA, Mao X, Nunez G, Thompson CB. bcl-x, a bcl-2-related gene that functions as a dominant regulator of apoptotic cell death. Cell 1993;74:597–608.
47. Aragon-Ching JB, Dahut WL. Chemotherapy in androgen-independent prostate cancer (AIPC): what's next after taxane progression? Cancer Ther 2007;5A:151–60.
48. Kadomatsu K, Muramatsu T. Midkine and pleiotrophin in neural development and cancer. Cancer Lett 2004;204:127–43.
49. Schiff PB, Horwitz SB. Taxol assembles tubulin in the absence of exogenous guanosine 5′-triphosphate or microtubule-associated proteins. Biochemistry 1981;20:3247–52.
50. Fang G, Chang BS, Kim CN, Perkins C, Thompson CB, Bhalla KN. "Loop" domain is necessary for taxol-induced mobility shift and phosphorylation of Bcl-2 as well as for inhibiting taxol-induced cytosolic accumulation of cytochrome c and apoptosis. Cancer Res 1998;58:3202–8.
51. Poruchynsky MS, Wang EE, Rudin CM, Blagosklonny MV, Fojo T. Bcl-xL is phosphorylated in malignant cells following microtubule disruption. Cancer Res 1998;58:3331–8.

Am J Physiol Heart Circ Physiol 296: H462–H469, 2009.
First published December 5, 2008; doi:10.1152/ajpheart.00733.2008.

Midkine prevents ventricular remodeling and improves long-term survival after myocardial infarction

Hiroharu Takenaka,[1,4]* Mitsuru Horiba,[4]* Hisaaki Ishiguro,[2,4] Arihiro Sumida,[4] Mayumi Hojo,[4] Akihiko Usui,[1] Toshiaki Akita,[1] Sadatoshi Sakuma,[5] Yuichi Ueda,[1] Itsuo Kodama,[4] and Kenji Kadomatsu[3]

Departments of [1]Cardiothoracic Surgery, [2]Cardiology, and [3]Biochemistry, Nagoya University Graduate School of Medicine; [4]Department of Cardiovascular Research, Research Institute of Environmental Medicine, Nagoya University, Nagoya; and [5]Cell Signals Incorporated, Yokohama, Japan

Submitted 15 July 2008; accepted in final form 18 November 2008

Takenaka H, Horiba M, Ishiguro H, Sumida A, Hojo M, Usui A, Akita T, Sakuma S, Ueda Y, Kodama I, Kadomatsu K. Midkine prevents ventricular remodeling and improves long-term survival after myocardial infarction. *Am J Physiol Heart Circ Physiol* 296: H462–H469, 2009. First published December 5, 2008; doi:10.1152/ajpheart.00733.2008.— Cardiac remodeling is thought to be the major cause of chronic heart dysfunction after myocardial infarction (MI). However, molecules involved in this process have not been thoroughly elucidated. In this study we investigated the long-term effects of the growth factor midkine (MK) in cardiac remodeling after MI. MI was produced by ligation of the left coronary artery. MK expression was progressively increased after MI in wild-type mice, and MK-deficient mice showed a higher mortality. Exogenous MK improved survival and ameliorated left ventricular dysfunction and fibrosis not only of MK-deficient mice but also of wild-type mice. Angiogenesis in the peri-infarct zone was also enhanced. These in vivo changes induced by exogenous MK were associated with the activation of phosphatidylinositol 3-kinase (PI3K)/Akt and MAPKs (ERK, p38) and the expression of syndecans in the left ventricular tissue. In vitro experiments using human umbilical vein endothelial cells confirmed the potent angiogenic action of MK via the PI3K/Akt pathway. These results suggest that MK prevents the cardiac remodeling after MI and improves the survival most likely through an enhancement of angiogenesis. MK application could be a new therapeutic strategy for the treatment of ischemic heart failure.

growth factor

ISCHEMIC HEART DISEASE (IHD) remains a leading cause of morbidity and mortality in many industrialized countries. Current treatment options for patients with advanced IHD include medical therapy or coronary revascularization by percutaneous coronary angioplasty or coronary bypass graft surgery (33). In a significant number of IHD patients, however, the standard revascularization therapies do not improve their clinical outcome. Induction of neovascularization by molecular biological procedures is expected to be a valid approach to ameliorate the pathophysiological changes in the ventricles of IHD. Transfer of angiogenic genes, cell implantation, and the administration of some growth factor proteins were reported to induce angiogenesis, leading to a prevention of cardiac fibrosis and resultant contractile dysfunction in animal IHD models (39). Most double-blind placebo-controlled clinical trials to date, however, failed to demonstrate sufficient efficacy of these procedures (11, 34).

Midkine (MK) is a heparin-binding growth factor with a molecular weight of 13 kDa, first isolated as the product of a retinoic acid-responsive gene in an embryonal carcinoma cell differentiation system, and is rich in basic amino acids and cysteine (15, 16). Structurally, MK shares ~50% sequence homology with pleiotrophin/heparin-binding growth-associated molecule (PTN/HB-GAM) but is not related to other growth factors or neurotrophic factors. The mouse MK and human MK have more than 90% homology (23), and human MK showed significant effects for mouse in vivo models (12, 13). MK has various biological activities; it promotes neurite outgrowth, survival of embryonic neurons, fibrinolytic activity of endotheial cells, and the migration of inflammatory leukocytes. MK is expressed strongly in early as well as advanced stages of tumors and involved in carcinogenesis and tumor progression. MK could have an angiogenic action on the ischemic heart because MK was shown to increase vascular density in tumorigenesis (4). The present study was designed to test this hypothesis in mouse models of myocardial infarction (MI). We have found that endogenous MK is responsible for adaptive angiogenesis in the heart after MI by regulating the activation of phosphatidylinositol 3-kinase (PI3K)/Akt and MAPKs. Exogenous application of MK was shown to improve cardiac function and survival of the post-MI mice through prevention of left ventricle (LV) remodeling. Notably, this improvement was observed not only in MK-deficient (MKKO) mice but also in wild-type (WT) mice.

MATERIALS AND METHODS

Mouse models. All animal experiments were performed in accordance with the regulations adopted by National Institutes of Health and approved by the Animal Care and Use Committee of Nagoya University. MKKO mice were generated as described elsewhere (25). Adult male C57BL/6 (WT) and male MKKO mice with the C57BL/6 genetic background were used in either ischemic-reperfusion or a ligation model of MI (age, 10–12 wk old; and weight, 22–25 g) and were fed normal rodent chow. Mice were anesthetized with pentobarbital (100 mg/kg ip) and ventilated through a nose cone with a tidal volume of 0.2 ml at 120 breaths/min using a rodent respirator (model SN-480-7; Shinano, Tokyo, Japan). The extremity leads of the ECGs were monitored continuously. A thoracotomy was performed in the left third intercostal space, and the beating heart was exposed. An 8-0 polypropylene suture was passed under the left coronary artery at the inferior edge of the left atrium and tied with a slipknot to

* H. Takenaka and M. Horiba contributed equally to this work.
Address for reprint requests and other correspondence: K. Kadomatsu, Dept. of Biochemistry, Nagoya Univ. Graduate School of Medicine, Tsurumai-cho, Showa-ku, Nagoya 466-8550, Japan (e-mail: kkadoma@med.nagoya-u.ac.jp).

The costs of publication of this article were defrayed in part by the payment of page charges. The article must therefore be hereby marked "*advertisement*" in accordance with 18 U.S.C. Section 1734 solely to indicate this fact.

produce occlusion. Myocardial ischemia was verified by blanching of the LV and ST elevation in ECGs. Air was then evacuated from the chest cavity, and the chest was closed with the ends of the slip outside of the incision. The ventilator was then removed, and normal respiration was restored. The blood samples of mice at 24 h after ischemic-reperfusion or the ligation procedure were collected from tail veins (0.2 ml each), and serum cardiac tropinin T (cTnT) levels were measured to estimate the initial MI size (SRL, Tokyo, Japan). The animals were euthanized 7–28 days after the surgical operation.

For the in vivo MK treatment experiments, MK protein in saline (1 mg/ml) was subcutaneously infused for 7–28 days by using an osmotic pump (Alza, Palo Alto, CA). As the control, saline was infused by the pump. The pumps were implanted under the abdominal skin and exchanged in each 7 days.

Histology. Mouse hearts were embedded in paraffin after fixation with 4% paraformaldehyde and were cut into 5-μm sections across the apex-base axis of the LV.

To recognize structural remodeling after MI, the sections were stained by both hematoxylin and eosin and picrosirius red. The amounts of collagen deposition (scar area) were estimated from six cross sections to cover the whole ventricles in each heart using automated image analysis software (Scion, Frederick, MD). Ten high-power fields per sample were analyzed, and the results were totaled for each animal.

Immunohistochemistry. Immunostaining of MK in paraffin sections was performed as described previously (12). Exposure to secondary antibody conjugated with goat anti-rat IgG (Jackson Laboratory, Bar Harbor, ME) was followed by incubation with biotinyl-tyramide and streptavidin-horseradish peroxidase (NEN Life Science Products, Boston, MA) to enhance the immunoreactive signals. The specificity of immunostaining for MK was confirmed by absorption of the anti-MK antibodies with recombinant MK, followed by heparin-sepharose affinity chromatography (12).

Immunohistochemical studies of von Willebrand factor (vWF) and CD31 were used to detect newly developed microvessels. The frozen sections (5-μm slices) were incubated overnight with the rat-anti-mouse vWF antibody (Santa Cruz, CA) or with the rat-anti-mouse CD31 antibody (BD Biosciences, Franklin Lakes, NJ) then exposed to the secondary antibody conjugated with goat anti-rat IgG (BD Biosciences). The images were analyzed by two investigators who were blinded with respect to the identification of the groups. The results were expressed as average numbers of capillaries per square millimeter.

Echocardiography. Transthoracic echocardiography was performed with a Nemio 20 (Toshiba Medical, Tokyo, Japan) to evaluate global cardiac function before and after MI creation. Mice were lightly anesthetized with diethyl ether and placed in the supine position on a heating pad. The level of anesthesia was kept very light to maintain regular spontaneous respiration and to avoid compromising hemodynamic conditions (13). A 12-MHz transducer was applied to the left hemithorax, and two-dimensional targeted M-mode tracings were recorded. The data were analyzed by an observer blinded to the treatment and genotype of mouse.

MK protein and antibodies. Human recombinant MK protein was generated and purified as previously described (12). Monoclonal antibodies against mouse MK were raised by injection of the purified protein into rabbits and were refined by affinity chromatography on protein-A and MK columns. Antibodies were specific to MK and did not react with PTN/HB-GAM.

Culture of human umbilical vein endothelial cells. Human umbilical vein endothelial cells (HUVEC) were purchased (Iwaki, Tokyo, Japan) and maintained according to an attached manual. Briefly, recovery cells were cultured at 37° in 5% CO_2-20% O_2 in 5% fetal bovine serum (FBS) supplemented with growth factors, 50 U/ml penicillin, and 50 μg/ml streptomycin. HUVEC at the third or fourth passage were used for the in vitro Matrigel assay and for the Western blotting.

Western blot analysis. Western blot analysis was performed to evaluate protein levels. LV tissue homogenates were subjected to SDS-PAGE on a 7.5% polyacrylamide gel, and proteins were electroblotted on polyvinylidene fluoride (PVDF) membranes (Atto, Tokyo, Japan). After blocking, the membrane was incubated with primary antibodies: anti-mouse Akt/PKB antibody (Upstate, Lake Placid, NY) anti-diphosphorylated Akt/PKB antibody (Upstate), PI3K (Upstate), anti-moue ERK antibody (Sigma) anti-diphosphorylated ERK1/2 antibody (NEN Life Science Products), hypoxia inducible factor (HIF)-1α (Bethyle, Montgomery, TX), JNK (Cell Signaling Technology, Boston, MA), P38 (Cell Signaling Technology), Bcl-2, Bad, and Bax (Santa Cruz Biotechnology, Santa Cruz, CA) and then exposed to biotinylated anti-mouse IgG (Sigma, St. Louis, MO), horseradish peroxidase-conjugated streptavidin (Amersham Pharmacia Biotech, Little Calfont, UK), and enhanced chemiluminescence reagent (Amersham Pharmacia Biotech).

To detect Akt and ERK1/2 proteins in vitro, cultured HUVEC were lysed in SDS sample buffer, the cell lysate was subjected to SDS-PAGE on a 7.5% polyacrylamide gel, and proteins were etectroblotted on PVDF membrane. The membrane was sequentially immunoblotted as described above. The intensity of the bands was quantified by densitometry (Atto).

Matrigel angiogenesis assays. For in vitro assay, the maintaining medium of confluent HUVEC was changed into 0.5% FBS in endothelial cell basal medium (EBM)-2 without supplemented growth factors. Twenty-four hours later, the medium was then aspirated and the cells were washed twice with phosphate-buffered saline (PBS), trypsinized, and plated in wells coated with growth factor-depleted Matrigel (Becton Dickison, Bedford, MA) (18) in 0.5% FBS in EBM-2 without growth factors. The HUVEC were then treated with either 100 ng/ml MK, 100 ng/ml basic FGF (bFGF; positive control), or PBS (control). At 6 h later, the palates were photographed, and the extent of tube formation was qualitatively assessed.

To assess the angiogenic efficacy in vivo, C57/BL6 mice were anesthetized with pentobarbital (100 mg/kg ip injection). The growth factor-depleted Matrigel was mixed with 20 U/ml heparin (Elkins Sinn, Cherry Hill, NJ) and either 500 ng/ml MK, 500 ng/ml bFGF (positive control), or PBS (control). Matrigel mixture (0.5 ml) was injected subcutaneously in the abdominal midline using sterile conditions. Fourteen days later, the pellets were then collected with a piece of underlying abdominal wall, fixed with paraformaldehyde for 2 h, and processed for paraffin embedding. The sections cut into 5 μm thickness were stained with hematoxylin and eosin or immunostained with an antibody against vWF. Images of sections at ×40 magnification were photographed with a digital camera and analyzed using automated image analysis software. Ten random high-power fields were analyzed, and the results were totaled for each animal.

Real-time PCR. To quantify mRNA expression of Syndecans (Assay ID: Sdc1 Mm00448918_m1, Sdc3 Mm01179832_m1, Sdc4 Mm00488527_m1), PI3K catalytic subunit p110 (Mm00440894_m1), Akt, monocyte chemoattractant protein (MCP)-1 (Ccl2 Mm00441242_m1), matrix metalloproteinases (MMP)-2(Mm00439508_m1) and MMP-9(Mm00600163_m1) in the LV free wall of mouse hearts and HUVEC, we performed a real-time PCR assay (Perkin-Elmer ABI Prism 7700) (27). 18s mRNA was used as an internal control. Sequence-specific probes were purchased from Applied Biosystems (Foster City, CA).

Statistic analysis. All values are expressed as means ± SE. Statistical comparisons among the groups were performed by ANOVA with Bonferroni post hoc tests. Comparisons between two groups were made using unpaired Student's *t*-test. The cumulative survival rate of mice after MI creation was analyzed by Kaplan-

Meier method with the long-rank procedure. Probability values of <0.05 were considered significant.

RESULTS

MK expression pattern in chronic phase. We evaluated the time course of MK expression after MI. The protein expression gradually increased, became apparent at 7 days, and persisted until 14 days (Fig. 1*A*, *top*). mRNA expression levels of MK were elevated from 3 days (4.0-fold; $P < 0.05$ vs. sham) to 14 days (7.2-fold; $P < 0.05$ vs. sham; Fig. 1*A*, *bottom*).

Survival rate after MI is improved by exogenous MK treatment. In MKKO mice, most animals (7 of 8) died by 7 days after MI, whereas the survival rate of WT mice was 44% at 28 days [WT with no treatment (WT-NT) in Fig. 1*B*]. Pump failure or ventricular rupture occurred more frequently in MKKO (5 of 7) than in WT (3 of 10) mice.

To examine the therapeutic potential of MK treatment after MI, we subcutaneously administered MK protein using an osmotic pump to MKKO mice. The survival rate of MKKO mice was significantly improved by supplemental treatment of MK protein [knockout (KO)-MK in Fig. 1*B*]. We further examined the effect of MK treatment on WT mice. At 24 h after MI, there was no significant difference of the serum cTnT level between WT-NT and MK treatment (WT-MK) groups (data not shown). Surprisingly, the survival rate was significantly improved to 90% by MK ($P < 0.05$; WT-MK in Fig. 1*B*). Consistent with this phenomenon, the serum brain natriuretic peptide (BNP) level at 28 days after MI in WT-MK mice was significantly lower than that of WT-NT (129 ± 5 pg/dl vs. 370 ± 98 pg/dl; $P < 0.05$; Fig. 1*C*).

MK treatment suppressed cardiac dysfunction and prevented progression of heart failure after MI. Figure 1*D* summarizes the parameters of echocardiography 7–28 days after MI. Without MK treatment (WT-NT), LV end-diastolic diameter (LVEDd) and LV end-systolic diameter (LVESd) were progressively increased, whereas ejection fraction (EF) and fractional shortening (FS) were progressively decreased during the entire follow-up period. This deterioration was prevented by MK treatment (WT-MK). LVEDd and LVESd at 28 days in WT-MK (4.3 ± 0.5 mm and 3.6 ± 1.0 mm) were significantly smaller than those in WT-NT (6.0 ± 0.4 mm and 5.3 ± 0.4 mm; $P < 0.05$). EF and FS at 28 days in WT-MK (44.3 ± 10.1% and 21.2 ± 5.4%) were significantly better than those in WT-NT (32.1 ± 0.6% and 15.3 ± 0.3%; $P < 0.05$).

Exogenous MK treatment inhibits LV remodeling and enhances neovascularization in WT mice after MI. To estimate LV remodeling, we first examined fibrosis. The area of collagen deposition quantified by picrosirius red staining at 28 days after MI in WT-MK was significantly smaller than that in WT-NT (Fig. 2*A*). Incidence of collagen deposition in WT-NT was expanded not only in the infarct zone but also in noninfarcted remote myocardium (Fig. 2*A*).

We next examined the gene expression of MMPs in the LV tissue. The MMP-9 mRNA level at 28 days after MI was significantly lower in WT-MK than in WT-NT (5.4 ± 1.82 vs. 2.2 ± 0.87; $P < 0.05$; Fig. 2*B*). The MMP-2 mRNA level at 28 days after MI in WT-MK tended to be lower than that in WT-NT although the difference did not reach a statistical significance (Fig. 2*B*).

Neovascularization was evaluated by means of immunohistochemistry. The CD31-immunopositive microvessel popula-

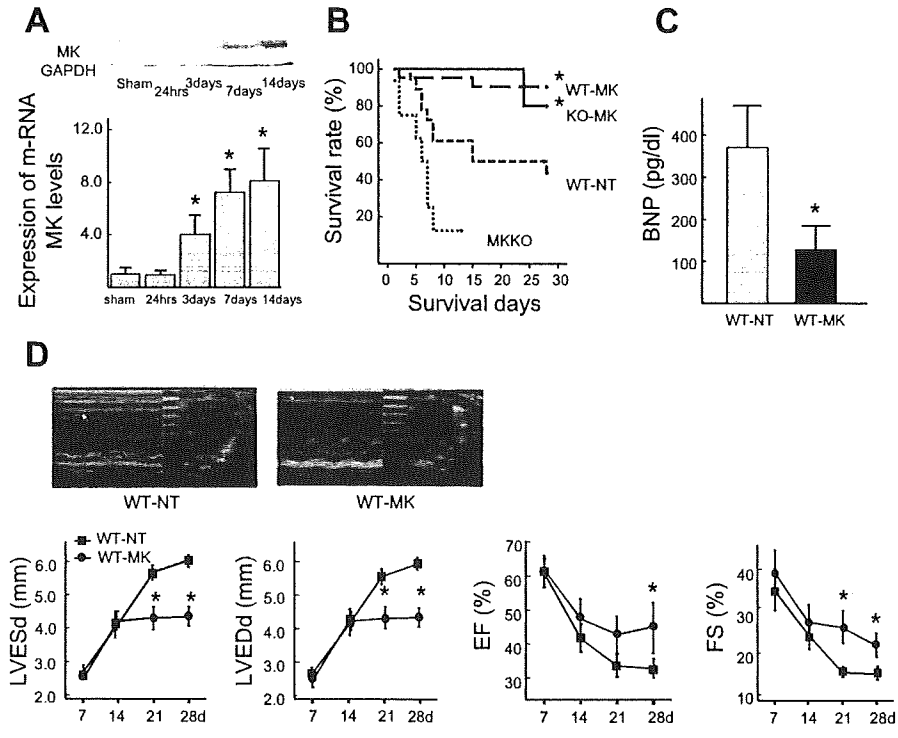

Fig. 1. Midkine (MK) expression pattern after myocardial infarction (MI) and consequences of MK treatment in terms of survival rate, serum brain natriuretic peptide (BNP), and echocardiographic assessments. *A*: protein expression of MK was identified by Western blotting in left ventricular (LV) tissue of wild-type (WT) mice. The photograph shown is a representative of 5 independent experiments. mRNA expression of MK (normalized to 18S) was measured by RT-PCR and summarized in the graph. *$P < 0.05$ vs. sham. *B*: survival rate estimated by Kaplan-Meier method in WT with no treatment (WT-NT; $n = 18$), WT treated with MK (WT-MK; $n = 21$), MK knockout mice (MKKO; $n = 8$), and MKKO treated with MK (KO-MK; $n = 5$). Survival rates of WT-MK and KO-MK were significantly higher than that of WT-NT ($P < 0.05$). *C*: serum BNP at 28 days (d) after MI. The values in WT-MK were significantly less than those of WT-NT ($n = 15$ each). *D*: LV end-diastolic diameter (LVEDd), LV end-systolic diameter (LVESd), ejection fraction (EF), and fractional shortening (FS) measured in echocardiography at 7, 14, 21, and 28 days after MI. Values are means ± SD of WT-NT ($n = 8$) and WT-MK ($n = 9$). LVEDd and LVESd in WT-MK at 21 and 28 days were significantly smaller than those in WT-NT. EF and FS in WT-MK at 28 days were significantly better than those in WT-NT. *$P < 0.05$ vs. WT-NT.

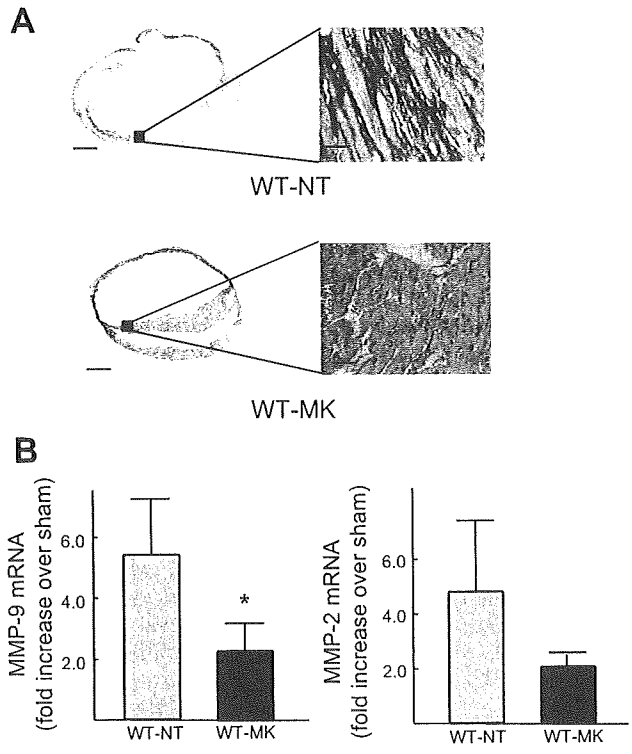

Fig. 2. Fibrosis and mRNA expression of matrix metalloproteinase (MMP)-2 and MMP-9 in ventricles at 28 days after MI. *A*: representative cross section of the ventricles in a WT-NT and WT-MK mouse stained by picrosirius red. The incidence of collagen deposition in the WT-MK was less expanding in the noninfarct area. Left scale bar, 2 mm; right scale bar, 50 μm. *B*: mRNA levels (normalized to 18S) of MMP-2 and MMP-9 in LV tissue after MI. MMP-9 mRNA in WT-MK (n = 3) was less than that in WT-NT (n = 4). Values are means ± SD; *P < 0.05 vs. WT-NT.

tion in the LV tissue at 28 days of WT-MK was significantly larger than that of WT-NT (79.2 ± 9.6 cells/mm^2 vs. 51.2 ± 9.4 cells/mm^2; P < 0.05; Fig. 3, *A* and *B*). To analyze the association between angiogenic phenomenon in WT-MK and proinflammatory action, we assessed transcript levels of MCP-1 in mouse LV tissue 7 days after MI. The expressions of MCP-1 mRNA in WT-MK were significantly higher than in WT-NT (1.35 ± .45 vs. 0.6 ± .17; P < 0.05; Fig. 3*C*).

To guarantee the above-mentioned protective effect of exogenous MK administration, administered MK must be properly delivered to the injured site of the heart. Figure 3*D* shows the localization of MK protein administered via an osmotic pump in a KO-MK mouse. The infused MK protein was localized in residual cardiomyocytes in the peri-infarct zone, and the MK accumulation area was roughly consistent with the CD31-enriched area.

Exogenous MK treatment enhances PI3K/Akt and MAPK signaling. Enhanced neovascularization by MK treatment prompted us to examine the expression of cell surface molecules (syndecans) and intracellular ones (PI3K, Akt, ERK, p38, and HIF-1α) that have relation to angiogenesis. The expressions of syndecans mRNA in LV tissue of WT-MK were significantly higher than in WT-NT 28 days after MI [syndecan-1 (Synd-1), 8.2 ± 4.0- vs. 3.2 ± 1.3-fold; syndecan-3 (Synd-3), 2.3 ± 0.7- vs. 1.2 ± 0.2-fold; and syndecan-4 (Synd-4), 1.4 ± 0.38 vs. 0.83 ± 0.2; P < 0.05. Values are normalized to sham] (Fig. 4).

Although there were no substantial differences of expressions of total PI3K and Akt between WT-MK and WT-NT, phosphorylation of PI3K (p-PI3K) and p-Akt was significantly increased in WT-MK (by 76.2% and 61.3%, respectively; P < 0.05) compared with WT-NT (Fig. 5*A*). Akt phosphorylation was remarkably reduced in the MKKO compared with WT at 24 h after MI (0.23 ± 0.09 vs. 0.9 ± 0.29; P < 0.05; Fig. 5*A*). p-Akt was localized in the microvessel area in WT-MK (Fig. 5*B*). The expression of p-ERK1/2 and p-p38 in WT-MK were significantly higher than in WT-NT (p-ERK1/2, 1.48 ± 0.75 vs. 0.57 ± 0.18; p-p38MAP, 1.98 ± 0.44 vs. 0.21 ± 0.054; P < 0.05; Fig. 5*C*).

Expression of the transcription factor HIF-1α was also examined. HIF-1α expression was remarkably increased in WT-MK (0.085 ± 0.041 vs. 0.028 ± 0.013; P < 0.05; Fig. 5*D*).

Exogenous MK treatment reduced apoptosis. The cellular consequence after MK administration was further evaluated as

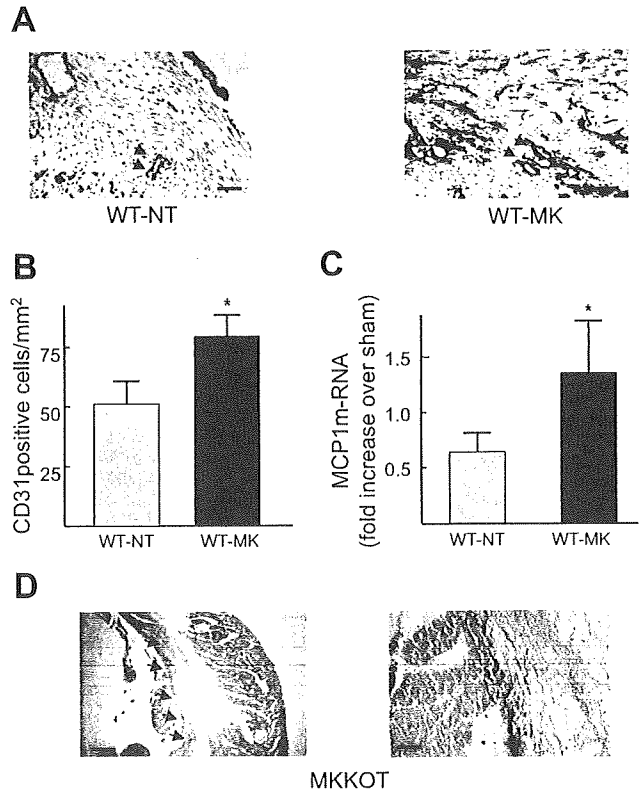

Fig. 3. Neovascularization and localization of infused MK in ischemic heart after MI. *A*: representative immunolabeling pictures for CD31 in LV free wall sections from a WT-NT and a WT-MK mouse 28 days after MI. Arrows indicate CD31-positive microvessels in the peri-infarct zone. Scale bar, 100 μm. *B*: density of CD31-positive capillaries in the peri-infarct zone. Values are means ± SE of WT-NT (n = 5) and WT-MK (n = 7). *P < 0.05 vs. WT-NT. The capillary density in WT-NT was significantly less than that of WT-MK. *C*: quantitative analysis of monocyte chemoattractant protein (MCP)-1 gene expression. The expression of mRNA (normalized to 18S) in WT-MK was significantly increased compared with that of WT-NT. *D*: localization of infused MK in the LV peri-infarct zone of a KO-MK mouse. Arrows indicate MK localization in the section of low (*left*) and high (*right*) magnification. Left scale bar, 100 μm; right scale bar, 50 μm. MKKOT, MKKO mouse treated with exogenous MK.

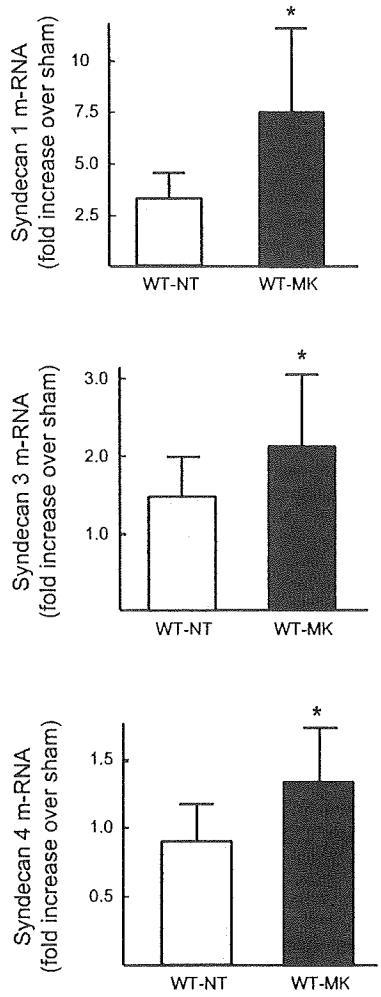

Fig. 4. Expressions of syndecans by MK treatment after MI. Quantitative analysis of syndecan-1, -3, and -4 mRNA expression (normalized to 18S) in the MK treatment hearts was significantly increased compared with that of WT-NT. The data are shown as means ± SD; *$P < 0.05$ vs. WT-NT.

to apoptotic changes in the LV tissue. Terminal deoxynucleotidyl transferase dUTP-mediated nick-end labeling (TUNEL)-positive cells were markedly decreased in WT-NT at 28 h after MI (Fig. 6*A*). The bax-to-bcl-2 expression ratio of the LV tissue in WT-MK was significantly suppressed compared with that of WT-NT (0.72 ± 0.37 vs. 1.46 ± 0.32; $P < 0.05$; Fig. 6*B*). p-Bad was significantly increased in WT-MK compared with WT-NT (1.0 ± 0.2 vs. 1.2 ± 0.2; $P < 0.05$; Fig. 6*C*).

Angiogenic activity of MK in Matrigel assay in vitro and in vivo. To confirm the ability of MK to enhance angiogenesis, we first examined the effect of exogenous MK on the formation of vascular structure of HUVEC in an in vitro Matrigel assay. Treatment of HUVEC with 100 ng/ml MK for 6 h resulted in a considerable acceleration of the formation of visible rings and cords of cells on growth factor-depleted Matrigel in the absence of serum. This enhancement of tubular network formation by MK was comparable with the effect of 100 ng/ml bFGF (Fig. 7*A*). We also examined the effect of MK on the activation of Akt in HUVEC by Western blotting (Fig. 7*B*). Treatment of HUVEC with 100 ng/ml MK for 6 h caused a significant increase of p-Akt (by 68.2% from control; $P < 0.05$), and this upregulation was reversed completely by the concomitant application of 30 nmol/l wortmannin, a specific inhibitor of PI3K. The network formation of HUVEC enhanced by MK was reversed by wortmannin (Fig. 7*A*).

To assess the angiogenic properties of MK in vivo, we measured the extent of vessel invasion into Matrigel pellets implanted in mouse abdominal walls. The incorporation of 500 ng/ml MK into the Matrigel resulted in a significant increase of vessels seen after 14 days compared with that of control pellets. The increase of capillary density by MK, which was measured by immunostaining for vWF in the pellets, was comparable with the effect of 100 ng/ml bFGF (Fig. 7, *C* and *D*).

DISCUSSION

The present study demonstrated that MK plays a crucial role in the cardiac remodeling after MI. Exogenous in vivo application of MK to WT mice after MI activated PI3K/Akt and MAPKs. Concomitantly, exogenous MK enhanced neovascularization in the peri-infarct zone, ameliorated LV fibrosis and dysfunction, and improved survival rate. Moreover, MKKO mice showed a higher mortality and less activation of Akt compared with WT mice. The angiogenic action of MK, which was associated with Akt activation, was confirmed in in vitro experiments using HUVEC. Taken together, these results suggest that MK exerts a protective effect against the ventricular remodeling after MI through the activation of angiogenesis.

Angiogenesis is the most important repair process of tissues subjected to ischemic insult, and stimulation of neovascularization is expected to reduce ventricular remodeling and dysfunction after MI (17, 36). The intracellular signaling molecules responsible for the neovascularization include PI3K/Akt and MAPKs (13, 24, 28). Among them, Akt is a serine/threonine protein kinase that is activated by a number of growth factors (e.g., VEGF, hepatocyte growth factor, and bFGF) in a PI3K-dependent manner. Akt regulates multiple critical steps in angiogenesis, including endothelial cell survival, migration, and capillary-like structure formation (32). HIF-1α exists downstream of Akt and regulates expression of many angiogenesis-related genes including those of VEGF and FLT (2, 9, 18, 20). It is of note that HIF-1α upregulates MK expression (30). Therefore, the potent angiogenic activity of MK as shown in the present experiments using mouse MI models would be explained primarily by the PI3K-Akt signaling axis like other growth factors. The marked reduction of Akt phosphorylation in MKKO mice suggested that MK has critical role to activate Akt, and indeed, exogenous treatment of MK for WT mice caused remarkable acceleration of Akt and PI3K activation after MI. In addition to these in vivo data, the in vitro action of exogenous MK on HUVEC to activate Akt and promote tubulogenesis was prevented by wortamannin, a specific inhibitor of PI3K.

Angiogenesis is deeply associated with inflammatory reaction (1). For instance, monocyte/macrophages accumulation is a critical player in both capillary sprouting and collateral artery growth. These inflammatory cells produce a variety of angiogenic cytokines and growth factors upon

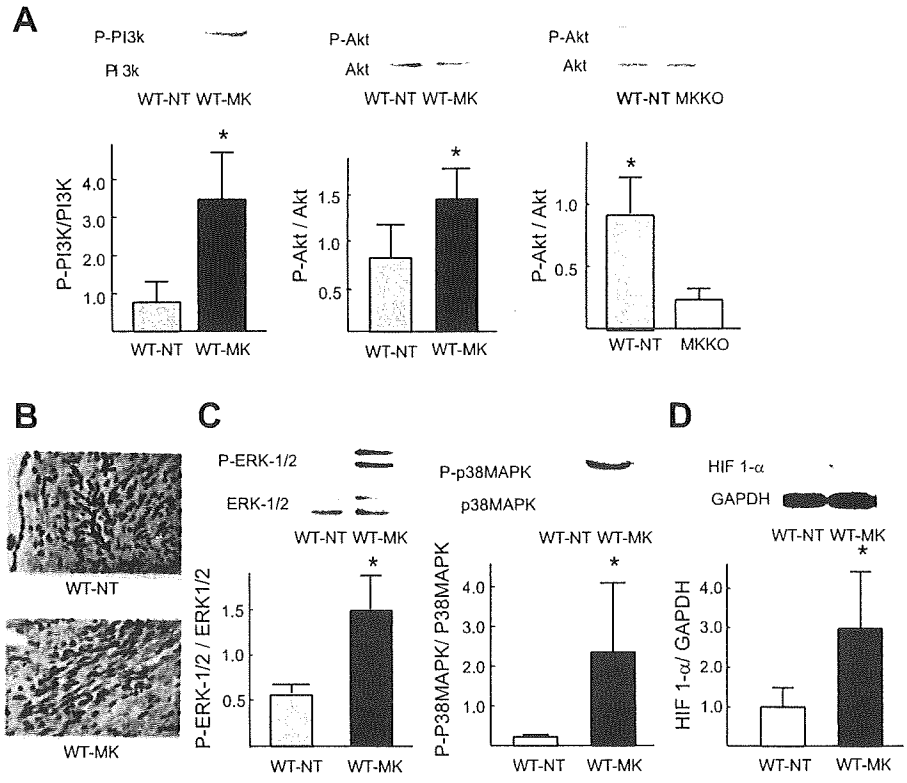

Fig. 5. Consequences of MK treatment in terms of phosphatidylinositol 3-kinase (PI3K)/Akt pathway, MAPK family, and hypoxia inducible factor (HIF)-1α expressions. *A*: Western blots of PI3K and Akt in LV at 28 days after MI. The amounts of phosphorylated (p) PI3K and p-Akt in WT-MK were significantly larger than those in WT-NT (n = 4 each). The expression of p-Akt in MKKO was significantly less than in WT-NT. Graphs are summaries of densitometric values. *B*: immunohistochemistry of p-Akt in WT-NT and WT-MK. Scale bar, 100 μm. *C*: representative Western blots showing ERK1/2 phosphorylation and p38 MAPK phosphorylation. Values are means ± SE (n = 4). *D*: expression of HIF-1α was significantly increased in WT-MK compared with WT-NT. *$P < 0.05$ vs. WT-NT. Arrows indicate microvessel area.

activation. MCP-1, TNF-α, bFGF, and MMPs belong to their repertoire (14, 37). In this study, the expression pattern of MK matched with the macrophage infiltration in acute or subacute inflammation phase after MI (14), and the survival rate of MKKO mice was significantly worse than WT in this phase (Fig. 1). From these data, there is a possibility that MK is also produced by inflammatory cells. In fact, Narita et al. (26) showed that MK is expressed by macrophages in neointima of hypercholesterolemic rabbits. On the other hand, MK is known to promote the chemotaxis of neutrophils or the migration of macrophages (12). Our laboratory has shown previously that MK has a critical role in neointima formation by enhancing the recruitment of inflammatory cells (12). MK also induces activation of MCP-1 and mediates the inflammatory reaction in the kidney subjected to ischemia-reperfusion (31). These observations suggest that the potent angiogenic activity of MK in the heart after MI is mediated in part by its proinflammatory action.

Is associated with an inflammatory reaction, which is a prerequisite for healing and scar formation. There is complex interplay among many factors involved in the reaction. In terms of LV remodeling and dysfunction after MI, inflammation can induce either undesirable or beneficial effects (10, 14). The former effect is the result of the progression of myocardial injury, whereas the latter one is the result mainly of an enhancement of angiogenesis, and the final consequence is determined by their balance under a variety of pathological conditions (7). Among MK-associated inflammatory molecules, MCP-1 has long been considered to play a deleterious role in postinfarct LV dysfunction and remodeling. Morimoto et al. (21), however, have shown in their study using transgenic mice that the cardioselective overexpression of MCP-1 prevents LV dysfunction and remodeling after MI through an enhancement of neovascularization.

We also found in the present study that the expression of syndecans was enhanced in MK-treated WT mice. Syndecans are membrane-bound heparan sulfated proteoglycans, and implicated in angiogenesis. For example, mice lacking Synd-4 show impaired angiogenesis, and Synd-2 is required for angiogenic spouting during zebrafish development (3, 6). It is interesting that MK binds to syndecans (6). Furthermore, a recent study by Vanhoutte et al. (35) using mice of targeted Synd1 deletion and adenovirus Synd1 gene overexpression has demonstrated that increased the expression of Synd-1 in MI prevents inverse healing, thereby reducing cardiac dilatation and dysfunction after MI. Accordingly, MK-induced syndecan family could contribute the amelioration of LV remodeling and dysfunction after MI through a similar mechanism. Beside syndecans, MK binds to other cell surface molecules. The MK receptor is thought to be a molecular complex including syndecan family members; protein-tyrosine phosphatase-ζ, a chondroitin sulfate proteoglycan; members of the low density lipoprotein receptor-related protein family; and anaplastic lymphoma kinase, a receptor-type tyrosine kinase (15, 19, 22, 24). Biological significance of these molecules after MI remains to be verified.

Fukui et al. (8) recently showed that MK has therapeutic effects for cardiac remodeling after MI. Although they did not show the detailed molecular mechanisms, the results were similar with our data in the point that the angiogenic

effect of MK showed preventive action for LV remodeling. In addition to their data, we have shown the involvement of the PI3K/Akt pathway in MK-mediated angiogenesis. Furthermore, the antiapoptotic effects of MK in MI model were demonstrated in the present study. We previously showed in mouse acute MI model induced by ischemia-reperfusion that MK ameliorates acute myocardial injury through its potent antiapoptoic action (13). In this study, we also found that MK treatment reduced apoptotic reaction in the chronic phase of ligation model. The signaling pathways of angiogenesis and apoptosis overlap and cross-talk each other: MAPKs especially initiate the activation of Bax and Bcl-2 (29). Bad, an proapoptotic member of the Bcl-2 family, is displaced by Bax from binding to Bcl-2 and Bcl-XL (38). In addition to MAPKs, the phosphorylated Akt inhibits the apoptotic effects of Bad (5). These facts suggest that the MK could prevent remaining myocardiocytes from apoptosis via MAPKs and Akt pathways. The potent angiogenic and antiapoptotic activities of MK in the chronic phase of MI may synergistically exert effects on the prevention of LV remodeling and dysfunction in favor of long-term survival. The beneficial effects of exogenous MK application would provide a new perspective for the innovation in the treatment of MI.

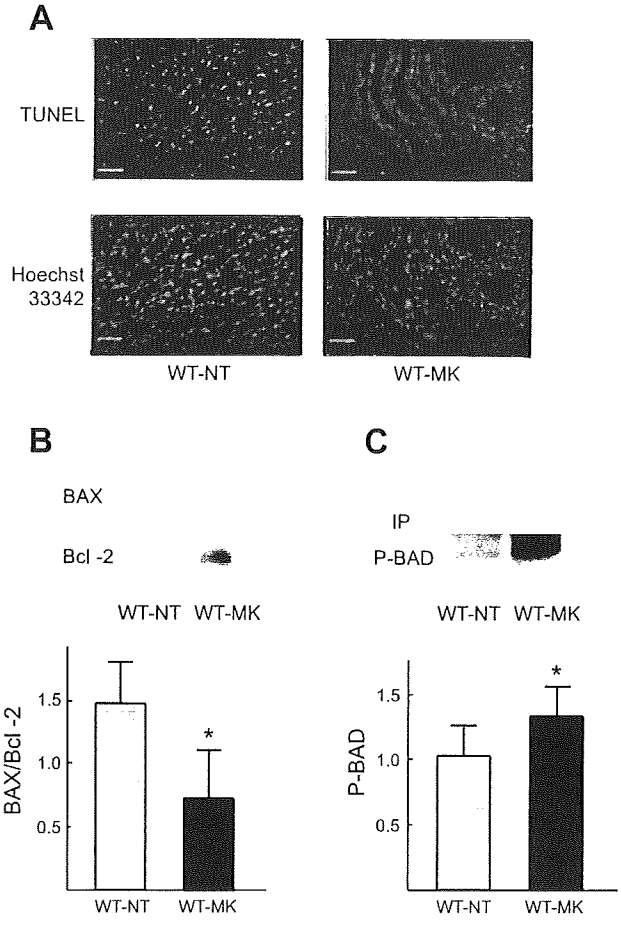

Fig. 6. Effects of apoptotic change in the postinfarct heart. *A*: terminal deoxynucleotidyl transferase dUTP-mediated nick-end labeling (TUNEL) staining in the peri-infarct area of WT-NT and WT-MK. WT-MK shows a marked decrease of TUNEL-positive apoptotic cells. *B*: representative Western blots of Bcl-2 and Bcl-2-associated X protein (Bax). The ratio of Bcl-2 to Bax in the WT-MK (n = 4) was significantly decreased compared with that in WT-NT (n = 4). *C*: representative Western blots of p-bcl-xl/bcl-2-associated death promoter (Bad). The p-Bad in the WT-MK (n = 4) was significantly increased compared with that in WT-NT (n = 4). Values are means ± SD. *P < 0.05 vs. WT-NT. Scale bars, 100 μm. IP, immunoprecipitation.

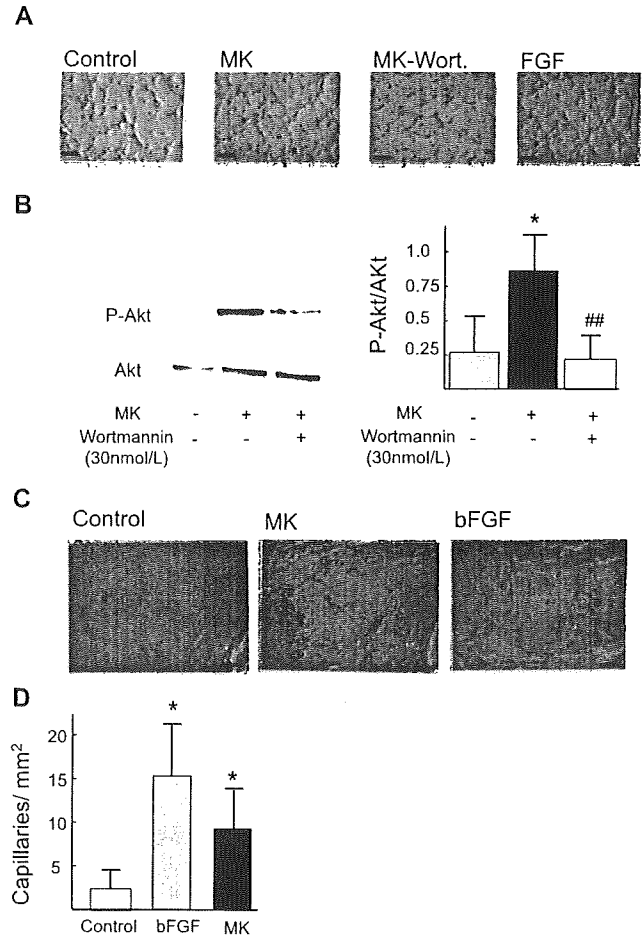

Fig. 7. Matrigel assays in vitro and vivo. *A*: in vitro assay to see the formation of vascular structure of human umbilical vein endothelial cells (HUVEC). HUVEC were seeded on growth factor-depleted Matrigel in the absence of serum and in the presence of either 100 ng/ml MK (n = 8), 100 ng/ml basic (b)FGF (positive control; n = 8), or vehicle (control; n = 6) and were photographed after 6 h. MK-treated and bFGF-treated cells showed much more extensive ring and cord formation than control cells. Scale bars, 50 μm. *B*: activation of Akt in HUVEC assessed by Western blots in Matrigel assay in vitro. Application of 100 ng/ml MK for 6 h caused a significant upregulation of p-Akt, and this upregulation was reversed by concomitant application of 30 nmol/l wortomannin (Wort; means ± SE, n = 5 each). *P < 0.01 vs. control. ##P < 0.01 vs. MK alone. *C*: in vivo assay is sections from control and MK- and bFGF-impregnated Matrigel pellets (hematoxylin and eosin). Treatment with either MK (500 ng/ml) or bFGF (100 ng/ml) resulted in a considerable increase in vessel invasion. Scale bar, 100 μm. *D*: density of newly formed vessels in Matrigel assessed by von Willebrand factor immunostaining (means ± SE; n = 10 each). *P < 0.05 vs. control.

ACKNOWLEDGMENTS

We thank Drs. H. Ohshima and M. Jijiwa for critical advice and S. Ikematsu for providing MK antibody. We thank T. Koike and A. Takahashi for technical assistance.

GRANTS

This work was supported by grants from the Ministry of Education, Culture, Sports, Science and Technology Japan (to M. Horiba).

REFERENCES

1. **Arras M, Ito WD, Scholz D, Winkler B, Schaper J, Schaper W.** Monocyte activation in angiogenesis and collateral growth in the rabbit hindlimb. *J Clin Invest* 101: 40–50, 1998.
2. **Carmeliet P, Dor Y, Herbert JM, Fukumura D, Brusselmans K, Dewerchin M, Neeman M, Bono F, Abramovitch R, Maxwell P, Koch CJ, Ratcliffe P, Moons L, Jain RK, Collen D, Keshert E.** Role of HIF-1 alpha in hypoxia-mediated apoptosis, cell proliferation and tumour angiogenesis. *Nature* 395: 525, 1998.
3. **Chen E, Hermanson S, Ekker SC.** Syndecan-2 is essential for angiogenic sprouting during zebrafish development. *Blood* 103: 1710–1719, 2004.
4. **Choudhuri R, Zhang HT, Donnini S, Ziche M, Bicknell R.** An angiogenic role for the neurokines midkine and pleiotrophin in tumorigenesis. *Cancer Res* 57: 1814–1819, 1997.
5. **Datta SR, Dudek H, Tao X, Masters S, Fu HA, Gotoh Y, Greenberg ME.** Akt phosphorylation of BAD couples survival signals to the cell-intrinsic death machinery. *Cell* 91: 231–241, 1997.
6. **Echtermeyer F, Streit M, Wilcox-Adelman S, Saoncella S, Denhez F, Detmar M, Goetinck PF.** Delayed wound repair and impaired angiogenesis in mice lacking syndecan-4. *J Clin Invest* 107: R9–R14, 2001.
7. **Frangogiannis NG, Smith CW, Entman ML.** The inflammatory response in myocardial infarction. *Cardiovasc Res* 53: 31–47, 2002.
8. **Fukui S, Kitagawa-Sakakida S, Kawamata S, Matsumiya G, Kawaguchi N, Matsuura N, Sawa Y.** Therapeutic effect of midkine on cardiac remodeling in infarcted rat hearts. *Ann Thorac Surg* 85: 562–570, 2008.
9. **Gerber HP, Condorelli F, Park J, Ferrara N.** Differential transcriptional regulation of the two vascular endothelial growth factor receptor genes. Flt-1, but not Flk-1/KDR, is up-regulated by hypoxia. *J Biol Chem* 272: 23659–23667, 1997.
10. **Giugliano GR, Giugliano RP, Gibson CM, Kuntz RE.** Meta-analysis of corticosteroid treatment in acute myocardial infarction. *Am J Cardiol* 91: 1055–1059, 2003.
11. **Henry TD, Annex BH, McKendall GR, Azrin MA, Lopez JJ, Giordano FJ, Shah PK, Willerson JT, Benza RL, Berman DS, Gibson CM, Bajamonde A, Rundle AC, Fine J, McCluskey ER.** The VIVA trial: Vascular endothelial growth factor in Ischemia for Vascular Angiogenesis. *Circulation* 107: 1359–1365, 2003.
12. **Horiba M, Kadomatsu K, Nakamura E, Muramatsu H, Ikematsu S, Sakuma S, Hayashi K, Yuzawa Y, Matsuo S, Kuzuya M, Kaname T, Hirai M, Saito H, Muramatsu T.** Neointima formation in a restenosis model is suppressed in midkine-deficient mice. *J Clin Invest* 105: 489–495, 2000.
13. **Horiba M, Kadomatsu K, Yasui K, Lee JK, Takenaka H, Sumida A, Kamiya K, Chen S, Sakuma S, Muramatsu T, Kodama I.** Midkine plays a protective role against cardiac ischemia/reperfusion injury through a reduction of apoptotic reaction. *Circulation* 114: 1713–1720, 2006.
14. **Jugdutt BI.** Ventricular remodeling after infarction and the extracellular collagen matrix: when is enough enough? *Circulation* 108: 1395–1403, 2003.
15. **Kadomatsu K, Muramatsu T.** Midkine and pleiotrophin in neural development and cancer. *Cancer Lett* 204: 127–143, 2004.
16. **Kadomatsu K, Tomomura M, Muramatsu T.** cDNA cloning and sequencing of a new gene intensely expressed in early differentiation stages of embryonal carcinoma cells and in mid-gestation period of mouse embryogenesis. *Biochem Biophys Res Commun* 151: 1312–1318, 1988.
17. **Krzeminski TF, Nozynski JK, Grzyb J, Porc M, Zeglen S, Filas V, Skopinska-Rozewska E, Sommer E, Filewska M.** Angiogenesis and cardioprotection after TNFalpha-inducer-Tolpa Peat Preparation treatment in rat's hearts after experimental myocardial infarction in vivo. *Vascul Pharmacol* 43: 164–170, 2005.
18. **Li J, Post M, Volk R, Gao Y, Li M, Metais C, Sato K, Tsai J, Aird W, Rosenberg RD, Hampton TG, Sellke F, Carmeliet P, Simons M.** PR39, a peptide regulator of angiogenesis. *Nat Med* 6: 49–55, 2000.
19. **Maeda N, Ichihara-Tanaka K, Kimura T, Kadomatsu K, Muramatsu T, Noda M.** A receptor-like protein-tyrosine phosphatase PTPzeta/RPTPbeta binds a heparin-binding growth factor midkine. Involvement of arginine 78 of midkine in the high affinity binding to PTPzeta. *J Biol Chem* 274: 12474–12479, 1999.
20. **Martin C, Yu AY, Jiang BH, Davis L, Kimberly D, Hohimer AR, Semenza GL.** Cardiac hypertrophy in chronically anemic fetal sheep: increased vascularization is associated with increased myocardial expression of vascular endothelial growth factor and hypoxia-inducible factor 1. *Am J Obstet Gynecol* 178: 527–534, 1998.
21. **Morimoto H, Takahashi M, Izawa A, Ise H, Hongo M, Kolattukudy PE, Ikeda U.** Cardiac overexpression of monocyte chemoattractant protein-1 in transgenic mice prevents cardiac dysfunction and remodeling after myocardial infarction. *Circ Res* 99: 891–899, 2006.
22. **Muramatsu H, Zou K, Sakaguchi N, Ikematsu S, Sakuma S, Muramatsu T.** LDL receptor-related protein as a component of the midkine receptor. *Biochem Biophys Res Commun* 270: 936–941, 2000.
23. **Muramatsu T.** Midkine (MK), the product of a retinoic acid responsive gene, and pleiotrophin constitute a new protein family regulating growth and differentiation. *Int J Dev Biol* 37: 183–188, 1993.
24. **Muramatsu T.** Midkine and pleiotrophin: two related proteins involved in development, survival, inflammation and tumorigenesis. *J Biochem (Tokyo)* 132: 359–371, 2002.
25. **Nakamura E, Kadomatsu K, Yuasa S, Muramatsu H, Mamiya T, Nabeshima T, Fan QW, Ishiguro K, Igakura T, Matsubara S, Kaname T, Horiba M, Saito H, Muramatsu T.** Disruption of the midkine gene (Mdk) resulted in altered expression of a calcium binding protein in the hippocampus of infant mice and their abnormal behaviour. *Genes Cells* 3: 811–822, 1998.
26. **Narita H, Chen S, Komori K, Kadomatsu K.** Midkine is expressed by infiltrating macrophages in in-stent restenosis in hypercholesterolemic rabbits. *J Vasc Surg* 47: 1322–1329, 2008.
27. **Niwa N, Yasui K, Opthof T, Takemura H, Shimizu A, Horiba M, Lee JK, Honjo H, Kamiya K, Kodama I.** Cav3.2 subunit underlies the functional T-type Ca^{2+} channel in murine hearts during the embryonic period. *Am J Physiol Heart Circ Physiol* 286: H2257–H2263, 2004.
28. **Qi M, Ikematsu S, Maeda N, Ichihara-Tanaka K, Sakuma S, Noda M, Muramatsu T, Kadomatsu K.** Haptotactic migration induced by midkine. Involvement of protein-tyrosine phosphatase zeta mitogen-activated protein kinase, and phosphatidylinositol 3-kinase. *J Biol Chem* 276: 15868–15875, 2001.
29. **Reddy KB, Nabha SM, Atanaskova N.** Role of MAP kinase in tumor progression and invasion. *Cancer Metastasis Rev* 22: 395–403, 2003.
30. **Reynolds PR, Mucenski ML, Le Cras TD, Nichols WC, Whitsett JA.** Midkine is regulated by hypoxia and causes pulmonary vascular remodeling. *J Biol Chem* 279: 37124–37132, 2004.
31. **Sato W, Yuzawa Y, Kadomatsu K, Tayasu T, Muramatsu H, Muramatsu T, Matsuo S.** Midkine expression in the course of nephrogenesis and its role in ischaemic reperfusion injury. *Nephrol Dial Transplant* 17 *Suppl* 9: 52–54, 2002.
32. **Shiojima I, Walsh K.** Role of Akt signaling in vascular homeostasis and angiogenesis. *Circ Res* 90: 1243–1250, 2002.
33. **Solomon AJ, Gersh BJ.** Management of chronic stable angina: medical therapy, percutaneous transluminal coronary angioplasty, and coronary artery bypass graft surgery. Lessons from the randomized trials. *Ann Intern Med* 128: 216–223, 1998.
34. **Unger EF, Goncalves L, Epstein SE, Chew EY, Trapnell CB, Cannon RO III, Quyyumi AA.** Effects of a single intracoronary injection of basic fibroblast growth factor in stable angina pectoris. *Am J Cardiol* 85: 1414–1419, 2000.
35. **Vanhoutte D, Schellings MW, Gotte M, Swinnen M, Herias V, Wild MK, Vestweber D, Chorianopoulos E, Cortes V, Rigotti A, Stepp MA, Van de WF, Carmeliet P, Pinto YM, Heymans S.** Increased expression of syndecan-1 protects against cardiac dilatation and dysfunction after myocardial infarction. *Circulation* 115: 475–482, 2007.
36. **Wang Y, Ahmad N, Wani MA, Ashraf M.** Hepatocyte growth factor prevents ventricular remodeling and dysfunction in mice via Akt pathway and angiogenesis. *J Mol Cell Cardiol* 37: 1041–1052, 2004.
37. **Yoshida S, Yoshida A, Ishibashi T.** Induction of IL-8, MCP-1, and bFGF by TNF-alpha in retinal glial cells: implications for retinal neovascularization during post-ischemic inflammation. *Graefes Arch Clin Exp Ophthalmol* 242: 409–413, 2004.
38. **Zha JP, Harada H, Yang E, Jockel J, Korsmeyer SJ.** Serine phosphorylation of death agonist BAD in response to survival factor results in binding to 14-3-3 not BGL-X(L). *Cell* 87: 619–628, 1996.
39. **Zhao XY, Hu SJ, Li J, Mou Y, Chan CF, Jin J, Sun J, Zhu ZH.** rAAV-mediated angiogenin gene transfer induces angiogenesis and modifies left ventricular remodeling in rats with myocardial infarction. *J Mol Med* 84: 1033–1046, 2006.

Xenotransplantation 2009: 16: 511–521
Printed in Singapore. All rights reserved
doi: 10.1111/j.1399-3089.2009.00549.x

Successful cross-breeding of cloned pigs expressing endo-β-galactosidase C and human decay accelerating factor

Yazaki S, Iwamoto M, Onishi A, Miwa Y, Suzuki S, Fuchimoto D, Sembon S, Furusawa T, Hashimoto M, Oishi T, Liu D, Nagasaka T, Kuzuya T, Maruyama S, Ogawa H, Kadomatsu K, Uchida K, Nakao A, Kobayashi T. Successful cross-breeding of cloned pigs expressing endo-β-galactosidase C and human decay accelerating factor. Xenotransplantation 2009; 16: 511–521. © 2009 John Wiley & Sons A/S.

Abstract: Background: For successful organ xenotransplantation, genetically engineered pigs have been actively produced. Our attention has focused on (i) reduction of αGal expression by its digestion enzyme, endo-β-galactosidase C (EndoGalC), and (ii) inhibition of complement activation by human decay accelerating factor (hDAF). Cell sorting and nuclear transfer enabled the effective production of cloned pigs expressing transgene at high levels. We report the successful cross-breeding of pigs expressing EndoGalC and hDAF.
Methods: After hDAF and EndoGalC genes were transfected into pig fibroblasts from the fetus of Landrace × Yorkshire and Meishan, respectively, transfected cells expressing transgenes effectively were collected using a cell sorter. Cloned pigs were produced using the technology of somatic cell nuclear transfer. After cross-breeding of cloned pigs, kidneys expressing both EndoGalC and hDAF were transplanted into baboons to examine the efficacy of gene transduction.
Results: Well-designed cloned pigs were produced by cross-breeding. αGal expression levels in cloned pigs were reduced up to 2 to 14%, compared to that in wild-type pigs. hDAF expression reached about 10- to 70-fold, compared to that in human umbilical vein endothelial cells. No congenital deformity was observed. There was no problem of increased stillbirth rate or growth retardation. Hyperacute rejection could be avoided in such a cloned pig to baboon kidney transplantation without any treatment for anti-pig antibody removal. However, grafts suffered from fibrin deposition as early as 1 h after transplantation, and were rejected after 1 week.
Conclusions: Using a cell sorting system for effective collection of transfected cells, two types of cloned pigs were produced with a very high level of hDAF expression and a low level of αGal expression. Such genetic modification was effective in preventing hyperacute rejection, but there was an immediate lapse into procoagulation after transplantation, resulting in acute vascular rejection. Effective suppression of antibody binding to the graft would be necessary, even if a high level of hDAF is expressed.

Satoko Yazaki,[1,2,*] Masaki Iwamoto,[1,2,*] Akira Onishi,[2] Yuko Miwa,[3] Shunichi Suzuki,[2] Dai-ichiro Fuchimoto,[2] Shoichiro Sembon,[2] Tadashi Furusawa,[2] Michiko Hashimoto,[1] Takatsugu Oishi,[1] DaGe Liu,[3] Takaharu Nagasaka,[4] Takafumi Kuzuya,[5] Shoichi Maruyama,[6] Haruko Ogawa,[7] Kenji Kadomatsu,[8] Kazuharu Uchida,[4] Akimasa Nakao[9] and Takaaki Kobayashi[3,9]

[1]Prime Tech Ltd, Tsuchiura, [2]Department of Developmental Biology, National Institute of Agrobiological Sciences, Tsukuba, [3]Department of Applied Immunology, Nagoya University School of Medicine, Nagoya, [4]Department of Transplant Surgery, Nagoya Daini Red Cross Hospital, Nagoya, [5]Department of Clinical Pharmacy, Nagoya University School of Medicine, Nagoya, [6]Department of Nephrology, Nagoya University School of Medicine, Nagoya, [7]Research Center for Animal Hygiene and Food Safety, Obihiro University of Agriculture and Veterinary Medicine, Obihiro, [8]Department of Biochemistry, Nagoya University School of Medicine, Nagoya, [9]Department of Surgery II, Nagoya University School of Medicine, Nagoya, Japan
*These authors contributed equally to this study.

Key words: cloned pig – crossbreeding – endo-β-galactosidase C – human DAF

Abbreviations: EndoGalC, endo-β-galactosidase C; αGal, Galα1, 3Gal; GT-KO, α1,3 galactosyltransferase knockout; hDAF, human decay accelerating factor; FITC, fluorescein isothiocyanate; FACS, fluorescence-activating cell sorting; GS-IB4, *griffonia simplicifolia* isolectin IB4; MFI, mean fluorescence intensity; CB, cytochalasin B; HUVEC, human umbilical vein endothelial cells; HAEC, human aortic endothelial cells; PAEC, porcine aortic endothelial cells.

Address reprint requests to Takaaki Kobayashi, Department of Applied Immunology, Nagoya University School of Medicine, 65 Tsurumai-cho, Showa-ku, Nagoya 466-8550, Japan
(E-mail: takakoba@med.nagoya-u.ac.jp)

Received 11 May 2009;
Accepted 4 August 2009

Introduction

In clinical application for xenotransplantation, which promises to overcome the mounting donor shortage, potent immune response must be totally controlled. The elimination of Galα1, 3Gal (αGal) antigens which had been considered to present the highest immunological barrier to successful pig to human xenotransplantation, has been realized by advanced clone technology, namely, successful production of α1,3 galactosyltransferase knockout (GT-KO) pigs [1–3].

However, graft injury has not been prevented completely even when organs from such GT-KO pigs were transplanted into non-human primates [4–7]. To obtain long-term graft survival, the indispensable key would be a novel strategy including gene transduction or knock-out (elimination) of other factors for donor pigs as well as effective treatment for recipients such as improvement of pharmacological immunosuppression and tolerance induction [8–11]. Several candidates for additional modifications proposed earlier include the regulation of complement, coagulation, costimulatory signal, and innate immunity such as NK and macrophage and infection [12,13]. Human regulatory protein such as human decay accelerating factor (hDAF, CD55), membrane co-factor protein (MCP, CD46) and CD59 has been considered to be one of the essential transgenes [14–17], because complement is related to cytotoxicity, inflammation, procoagulation and immune response, and becomes a strong initiator for endothelial activation, leading to graft injury immediately after antibody binding or independently of it [18–20].

The first step in achieving genetically engineered pigs for xenotransplantation was the introduction of human DAF (CD55), which was a landmark because of the drastic improvement in graft survival over 3 months [21]. We previously reported the usefulness of high expression of hDAF in pig cells (over 15-fold higher than human endothelial cells), which showed a high ability to prevent the cytotoxicity of human sera [22]. Subsequently, we have made it possible to produce cloned pigs with such high hDAF expression using a cell sorter, which allowed the collection of hDAF highly expressed fibroblasts for nuclear transfer.

In developing a strategy to eliminate αGal expression, we originally directed our attention to the digestion of αGal epitopes using the enzyme, called endo-β-galactosidase C (EndoGalC) [23]. After that, GT-KO pigs were proven to be successfully produced. However, the production of cloned GT-KO pigs has been feasible in a limited number of institutions, because gene knock-out (elimination) in pigs requires cutting-edge technology and a robust budget, compared to gene introduction. To explore the possibility of EndoGalC gene transfer as an alternative and additional strategy to GT-KO, we have continued to produce cloned pigs expressing EndoGalC, according to promising evidence which showed that an in vitro test of gene transfer of EndoGalC demonstrated almost complete removal of αGal expression from pig cells [24].

Next, cross-breeding of pigs expressing hDAF and EndoGalC has been attempted, resulting in the establishment of genetically engineered pigs effectively expressing both hDAF and EndoGalC genes. We have examined the usefulness of the pig graft with a high level of hDAF expression and EndoGalC-induced αGal reduction.

In this study, we report the successful cross-breeding of pigs expressing hDAF and EndoGalC, and the effectiveness and limitation of such gene transduction in a pig to baboon kidney transplantation model.

Materials and methods

Animals

In connection with the production of genetically engineered pigs, all procedures were carried out in accordance with National Institute of Agrobiological Sciences after approval by the Japanese Ministry of Education, Culture, Sports, Science and Technology. Breeding and transfer of the produced genetically engineered pigs complied with the Cartagena protocol domestic law.

The pigs and baboons used in this study received humane care in compliance with the Guide for the Care and Use of Laboratory Animals prepared by the National Academy of Sciences and published by the National Institutes of Health. Experimental protocols for clone pig to baboon kidney transplantation were approved by the Committee on Research Animal Care, Institute for Laboratory Animal Research, Nagoya University School of Medicine.

Preparation of donor cells expressing hDAF for nuclear transfer

Pig fibroblasts which were obtained from the fetus of Landrace × Yorkshire as described previously [25] were used for hDAF gene transfer. hDAF cDNA was subcloned into the pCAGGS expression cassette (pCAG–hDAF-p(A)) that contains the cytomegalovirus enhancer, chicken β-actin promoter, and a portion of the second intron [26]. Next, a puromycin-resistance gene cassette (PGK-puro-p(A)) was ligated to the terminal

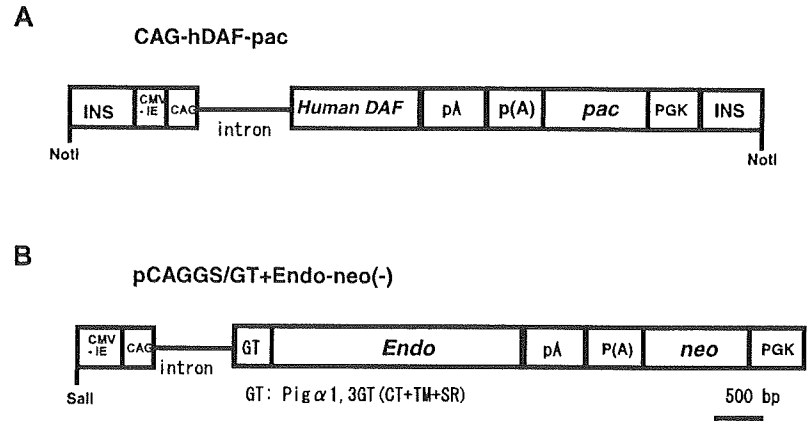

Fig. 1. Vector constructs. (A) hDAF expression vector; (B) EndoGalC expression vector. hDAF, human decay accelerating factor; Endo, endo-β-galactosidase C; CMV-IE, Cytomegalovirus immediate-early 1 gene enhancer; CAG, Chicken β-actin promoter; pA, Rabbit β-globin polyA; PGK, Mouse phosphoglycerate kinase 1 promoter; *pac*, Puromycin resistant gene; *neo*, Neomycin-resistant gene; p(A), Mouse phosphoglycerate kinase 1 poly(A) signal; CT, Cytoplasmic tail; TM, Transmembrane domain; SR, Stem region; INS, Sea urchin ARS insulator.

region of the pCAGGS expression cassette. Sea Urchin Ars insulator gene was then outwardly ligated to the two ends of the cassettes, and hDAF expression vector (pOL-CAGhDAF-pac) was completed (Fig. 1A). hDAF expression vector was introduced into fetal fibroblasts by Lipofectamine PLUS Reagent (Invitrogen, Carlsbad, CA, USA). After puromycin selection (1.0 to 2.0 μg/ml) for 7 days and cell culture for 2 weeks, fibroblasts were subjected to fluorescence-activating cell sorting (FACS) (EPICS ALTRA Multi-COMP; Beckman Coulter, Fullerton, CA, USA). Cells stained with fluorescein isothiocyanate (FITC)-conjugated anti-CD55 (hDAF) antibody at a high level were collected by gating on fluorescence intensity (Fig. 2A). Only fibroblasts expressing hDAF at a high level were used for nuclear transfer.

Preparation of donor cells expressing EndoGalC for nuclear transfer

Pig fibroblasts obtained from the fetus of Meishan as described previously [25] were used for EndoGalC gene transfer. We earlier reported that EndoGalC digests the linkage between Gal β1-4 GlcNAc in Gal epitopes and that the gene introduction effectively reduced αGal expression in pig cells [24,27]. pCAGGS/GT + EndoGalC expression cassette was prepared as described previously [24]. Next, an inverted neomycin-resistance gene cassette (PGK-neo-p(A): neo(−)) was ligated to the terminal region of the pCAGGS expression cassette and pCAGGS/GT + EndoGalC-neo(−) expression vector was completed (Fig. 1B). Fetal somatic cells were electroporated in 500 μl of HEPES-buffered saline containing 5 nM of pCAGGS/GT + EndoGalC-neo(−) expression vector using an electroporation system (Gene Pulser II; Bio-Rad Co. Ltd., Hercules, CA, USA) with 750 V/cm, 950 μF one pulse. Electroporated cells were then cultured in a 100-mm plastic dish (#3003; Becton Dickinson, Franklin Lakes, NJ, USA) with 10 ml of Dulbecco's Modified Eagle's Medium (DMEM) (D5796; Sigma-Aldrich, St. Louis, MO, USA) containing 10% fetal bovine serum at 37 °C in a humidified atmosphere of 5% CO_2 in air. After 24

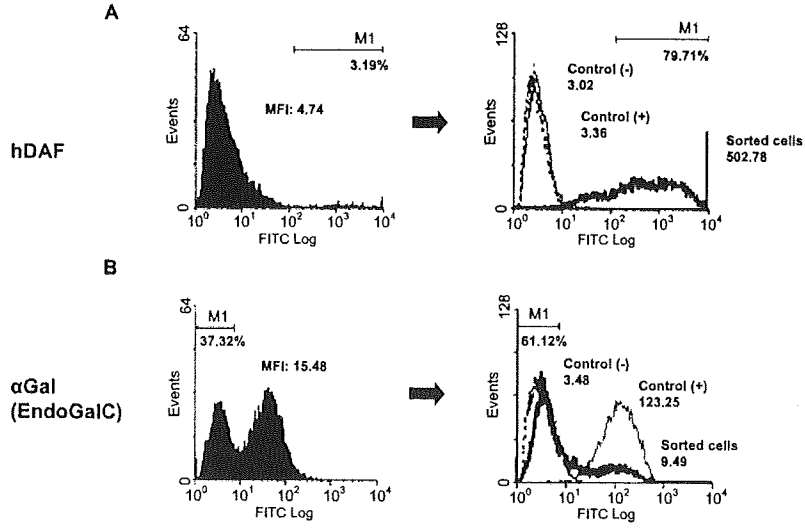

Fig. 2. Flow cytometric analysis before and after cell sorting. (A) hDAF-expressed fibroblasts; (B) EndoGalC-expressed fibroblasts. Left: before cell sorting; right: after cell sorting. Control (+) and control (−) indicate wild-type pig fibroblasts with and without the staining of FITC-labeled antibody. Transfected cells were sorted within the range of M1 by FACS. Sorted cells are indicated by thick lines. MFI, mean fluorescence intensity.

to 48 h in culture, 500 to 800 μg/ml of neomycin was added to the medium for selection of cells carrying pCAGGS/GT+ EndoGalC-neo(−) for 10 days. These surviving cells were grown to confluence and stained with FITC-labeled *Griffonia simplicifolia* isolectin IB4 (GS-IB4) which recognizes αGal, and subjected to FACS (EPICS ALTRA Multi-COMP). The mean fluorescence intensity (MFI) was used to quantitate the expression level of αGal. Therefore, cells stained with GS-IB4 at a low level could be surmised to be expressing EndoGalC at a high level and collected by gating on fluorescence intensity (Fig. 2B). Only fibroblasts expressing αGal at a low level were used for nuclear transfer.

Production of cloned pigs expressing hDAF and EndoGalC

Cloned piglets expressing hDAF and EndoGalC were produced by nuclear transfer as described previously [25]. Moreover, in vivo and in vitro mature oocytes (metaphase II oocytes) used for somatic cell nuclear transfer were prepared as described previously [25,28]. Metaphase II oocytes were enucleated by gentle aspiration of the first polar body and adjacent cytoplasm using a beveled pipette (25 to 30 μm) in PZM3 medium [29] containing 5.0 μg/ml cytochalasin B (CB). After enucleation, oocytes were washed in PZM3 without CB. Nuclei of transgenic donor cells were transferred into the enucleated oocytes by direct intracytoplasmic injection using a piezo-actuated micromanipulator (Prime Tech., Tsuchiura, Japan) in accordance with the method described previously [25,28,30]. Oocytes injected with donor cell nuclei were transferred to activation solution consisting of 0.28 M *d*-mannitol, 0.05 mM $CaCl_2$, 0.1 mM $MgSO_4$, and 0.01% (w/v) bovine serum albumin (BSA; Sigma, St. Louis, MO, USA), and washed once. The oocytes were then stimulated with a direct current pulse of 1.5 kV/cm for 100 μs using a somatic hybridizer (SSH-10; Shimadzu, Kyoto, Japan). They were then transferred for 2 h to PZM3 supplemented with CB to prevent extrusion of a pseudo-second polar body. The reconstructed (nuclear transferred) oocytes were then cultured in PZM3 medium in an atmosphere of 5% CO_2, 5% O_2, and 90% air at 38.5 °C for 2 days until the two- to eight-cell stage. The cleaved embryos were transferred to the oviducts (200 embryos per a surrogate) of an anesthetized surrogate mother (mature LWD; Landrace × Large White × Duroc crosses). Embryo transfer was performed nine times using 11 surrogates for the embryos derived from nuclear transfer of hDAF expressing cells. Similarly, embryo transfer was performed seven times using seven surrogates for the embryos derived from nuclear transfer of EndoGalC expressing cells. These surrogate mothers were previously pregnant by artificial insemination after injection of superovulation inducing hormones and artificially aborted. After embryo transfer, these mothers were kept under a conventional environment employed for housing pigs and observed daily for confirmation of pregnancy by checking estrus. All of the transgenic cloned piglets were delivered on day 113 to 116 of gestation without labor induction.

Cross-breeding of cloned pigs expressing hDAF and EndoGalC

For preservation of progeny and analysis of transgene expression, fibroblasts were obtained from the ear after birth and cultured in DMEM supplemented with 10% FCS. The course of cross-breeding of cloned pigs expressing hDAF and EndoGalC was depicted in Fig. 7. Meishan female pig expressing EndoGalC founder was bred with a Large White × Landrace male pig expressing hDAF to produce the F1 generations. Close attention was paid to the following cross-breeding in the light of the preservation of genetic variation as much as possible and the minimization of any problems associated with inbreeding depression in subsequent generation.

Flow cytometry

The efficacy of transgene was evaluated by flow cytometry. Cultured fibroblasts obtained from the piglet's ear were examined for evaluation of the expression level of hDAF and αGal antigens. Aortic endothelial cells harvested from euthanized cloned piglets or stillborn neonate were also examined for evaluation. For the detection of hDAF and αGal antigen, FITC-labeled anti-CD55 (hDAF) antibody (BD Biosciences, San Jose, CA, USA) and FITC-labeled GS-IB4 (Sigma) were used as mentioned above. The expression level of hDAF was described as a relative value of human positive control, which was calculated by MFI.

Human umbilical vein endothelial cells (HUVEC) and human aortic endothelial cells (HAEC) (Lonza Corporation, Walkersville, MD, USA) were used as a positive control at low passage number (below 7) to avoid instability of expression pattern and change of character. Fibroblasts and aortic endothelial cells (PAEC) obtained from wild-type newborn pigs were used as a negative control for hDAF expression and as a positive control for αGal expression. The expression level of αGal